Table S1. Antibodies

Antigen	Name	Company
Immunohistochemistry		
CDH1	Alexa fluor 647-conjugated rat anti-human CD324 (E-cadherin) Rat anti-human CD324 (E-cadherin)	eBioscience (clone DECMA-1)
EPCAM	Allophycocyanin (APC)-conjugated rat anti-mouse CD326 (EpCAM) Rat anti-mouse CD326 (EpCAM)	BioLegend (clone G8.8)
KIT	APC-conjugated rat anti-mouse CD117 (c-kit) Rat anti-mouse CD117 (c-kit)	eBioscience (clone ACK2)
FBXW7	Rabbit anti-human Fbxw7	Lifespan Biosciences (LS-B2909)
MKI67	Alexa fluor 488-conjugated mouse anti-human K_i-67	BD Biosciences (clone B56)
SYCP3	Rabbit anti-human Sycp3	Abcam (ab15093)
GATA4	Rabbit anti-human GATA4	Abcam (ab84593)
MYC	Rabbit anti-human c-Myc	Santa Cruz Biotechnology (sc-764)
CCNE1	Rabbit anti-rat cyclin E1	Santa Cruz Biotechnology (sc-481)
CDK4	Rabbit anti-mouse CDK4	Abcam (ab7955)
CDC25A	Rabbit anti-human CDC25A	Lifespan Biosciences (LS-B1463)
CDKN2A	Rabbit anti-mouse CDKN2A/p19 ARF	Abcam (ab80)
Secondary reagents		
Alexa fluor 488-conjugated goat anti-rabbit IgG		Invitrogen (cat. no. A11008)
Alexa fluor 568-conjugated goat anti-rabbit IgG		Invitrogen (cat. no. A11011)
Alexa fluor 647-conjugated goat anti-rabbit IgG		Invitrogen (cat. no. A21245)
Alexa fluor 647-conjugated goat anti-rat IgG		Invitrogen (cat. no. A21247)
Flow cytometry		
KIT	APC-conjugated rat-anti-mouse c-kit	eBioscience (clone ACK2)
EPCAM	Rat anti-mouse EpCAM	BioLegend (clone G8.8)
ITGA6	Rat anti-mouseCD49f (α6-integrin)	BD Biosciences (clone GoH3)
ITGB1	Biotin-conjugated hamster anti-rat CD29 (β1-integrin)	BD Biosciences (clone Ha2/5)
GFRA1	Biotin-conjugated goat anti-rat Gfrα1	R&D systems (BAF560)
NOTCH1	Biotin-conjugated goat anti-mouse Notch1	BioLegend (HMN1-12)
NOTCH2	APC-conjugated hamster anti-mouse Notch2	BioLegend (HMN2-35)
Secondary reagents		
Alexa fluor 647-conjugated hamster IgG isotype control		BioLegend (clone HTK888)
APC-conjugated Streptavidin		eBioscience (17-4317)
APC-conjugated goat anti-rat IgG+IgM		BD Bioscience (551019)
Western blotting		
FBXW7	Rabbit anti-human Fbxw7	Lifespan Biosciences (LS-B2909)
MYC	Rabbit anti-human c-Myc	Santa Cruz Biotechnology (sc-764)
MYCN	Rabbit anti-human *N*-Myc	Cell Signaling (9405)
CCNE1	Rabbit anti-rat cyclin E1	Santa Cruz Biotechnology (sc-481)
Phosphorylated JUN	Rabbit anti-human phospho-c-Jun (Ser63) II	Cell Signaling (9261)
MCL1	Rabbit anti-human Mcl-1	Abcam (ab32087)
KLF5	Rabbit anti-human Klf5	Abcam (ab137676)
MTOR	Rabbit anti-human mTOR	Cell Signaling (2972)
SREBF1	Rabbit anti-human Srebp1	Santa Cruz Biotechnology (sc-367)
ACTB	Mouse anti-β-actin antibody	Sigma (clone AC-15)
CCND1	Mouse anti-human cyclin D1	Cell Signaling (2926)
CCND2	Rabbit anti-cyclin D2	Cell Signaling (2924)
CCND3	Mouse anti-human cyclin D3	Cell Signaling (2936)
Phosphorylated MAPK14	Rabbit anti-human phospho-p38 MAPK (Thr180/Tyr182)	Cell Signaling (4511)
Phosphorylated MAP2K1	Rabbit anti-human phospho-MEK1/2 (Ser217/221)	Cell Signaling (9121)
Phosphorylated AKT	Rabbit anti-human phospho-Akt (Ser473)	Cell Signaling (9271)
CDKN2B	Rabbit anti-human CDKN2B (p15)	Cell Signaling (4822)
CDKN2A	Rat anti-mouse CDKN2D (p19)	Santa Cruz Biotechnology (sc-32748)
NICD1	Rabbit anti-activated human Notch1	Abcam (ab8925)
NICD2	Rabbit anti-human Notch2 intracellular domain	Abcam (ab52302)
Secondary reagents		
HRP (horseradish peroxidase)-conjugated horse anti-mouse IgG		Cell Signaling (cat. no. 7076)
HRP-conjugated horse anti-rabbit IgG		Cell Signaling (cat. no. 7074)
HRP-conjugated goat anti-rat IgG + IgM		Jackson Immunoresearch (112-035-044)

Table S2. KD vectors

Gene	Vector
Taf4b	TRCN0000241312
Zbtb16	TRCN0000012941
Foxo1	TRCN0000054878, TRCN0000054879, TRCN0000054880, TRCN0000054881, TRCN0000054882
Id2	TRCN0000054388, TRCN0000054389, TRCN0000054390
Id3	TRCN0000071438, TRCN0000071439, TRCN0000071440
Id4	TRCN0000071444
Gilz	TRCN0000085743, TRCN0000085744, TRCN0000085745, TRCN0000085746, TRCN0000085747
Myc	TRCN0000042513, TRCN0000042514, TRCN0000042515, TRCN0000042516
Mycn	TRCN0000042523, TRCN0000042525, TRCN0000042526, TRCN0000042527
Ccne1	TRCN0000077775, TRCN0000077776, TRCN0000077777
Ccne2	TRCN0000077779, TRCN0000077780, TRCN0000077781, TRCN0000077782
Pin1	TRCN0000012579, TRCN0000012580
Skp2	TRCN0000088758, TRCN0000088759, TRCN0000088760, TRCN0000088761, TRCN0000088762
Kpc1	TRCN0000201178, TRCN0000201651, TRCN0000192171, TRCN0000200959, TRCN0000191626
Rbpj	TRCN0000097286, TRCN0000097287, TRCN0000097288

Table S3. PCR primers and genotyping

Genotyping		
Fbxw7	Forward: TGGTATAGGCTTAACCCTATAGGG	
	Reverse: AGCCATCTACTCTCACTCACAG	
	WT, 650 bp; Flox, 900 bp	
R26R	IMR0315: GCGAAGAGTTTGTCCTCAACC	
	IMR0316: GGAGCGGGAGAAATGGATATG	
	IMR0883: AAAGTCGCTCTGAGTTGTTAT	
	WT, ~600 bp; Flox, ~300 bp	
	Forward	Reverse
RT-PCR		
Stra8	AACGGTATCTCAACTTTTACAAGCA	ATTTCTCCTCTGGATTTTCTGAGTT
Hoxa4	TGAGCGCTCTCGAACCGCCTATACC	GATGGTGGTGTGGGCTGTGAGTTTG
Crem	GATTGAAGAAGAAAAATCAGA	CATGCTGTAATCAGTTCATAG
Piwil1	ATGATCGTGGGCATC	AGGCCACTGCTGTCATA
Clgn	ATATGCGTTTCCAGGGTGTTGGAC	GTATGCACCTCCACAATCAATACC
Sycp3	GGTGGAAGAAAGCATTCTGG	CAGCTCCAAATTTTTCCAGC
Prm	ACGAAGATGTCGCAGACGGAGGAG	CATCGGCGGTGGCATTTTTCAAGA
Hprt	GCTGGTGAAAAGGACCTCT	CACAGGACTAGAACACCTGC
qPCR		
Hprt	GCTGGTGAAAAGGACCTCT	CACAGGACTAGAACACCTGC
Fbxw7	TGCAAAGTCTCAGATTATACC	ACTTCTCTGGTCCGCTCCAGC
Fbxw7α	CTCACCAGCTCTCCTCTCCATT	GCTGAACATGGTACAAGGCCA
Fbxw7β	AGAAAATATGGGTTTCTACGG	TTGCTGAACATGGTACAAGG
Fbxw7γ	AACCATGGCTTGGTTCCTGTTG	CAGAACCATGGTCCAACTTTC
Taf4b	AGATGTTACTAAAGGCAGCC	GCAAGCTCCAACTGCTGCAA
Zbtb16	CACACTCAAGAGCCACAAGC	ATCATGGCCGAGTAGTCTCG
Foxo1	GTGAAGAGCGTGCCCTACTT	TCCTTCATTCTGCACTCGAA
Id2	ACTATCGTCAGCCTGCATCA	AGCCACAGAGTACTTTGCTA
Id3	TCGGAACGTAGCCTGGCCAT	TGGCTAAGCTGAGTGCCTCG
Id4	GTTCACGAGCATTCACCGTA	AAGGTTGGATTCACGATTGC
Gilz	CCCTAGACAACAAGATTGAGC	CTTCTCAAGCAGCTCACGAA
Pin1	AGATCACCAGGAGCAAGGAG	TGAACTGTGAGGCCAGAGAT
Skp2	GCAAAGGGAGTGACAAAGAC	TCCCAAGGAGCAGCTCATCT
Kpc1	CTCAGATGCTGAGAAGTCCA	AGTTTAGCGGTTTCCTGCTG
Cdkn2b	CAGATCCCAACGCCCTGAAC	GCAGTTGGGTTCTGCTCCGT
Cdkn2a(p16)	ACATCAAGACATCGTGCGA	TAGCTCTGCTCTTGGGATTG
Cdkn2a(p19)	GGTTCTGGTCACTGTGAGG	TGAGCAGAAGAGCTGCTACG
Cdkn1a	GCAGATCCACAGCGATATCC	CAACTGCTCACTGTCCACGG
Cdkn1b	AGGAGAGCCAGGATGTCAGC	GAATCTTCTGCAGCAGGTCG
Rbpj	AGCTGAACTTGGAAGGGAAG	CGCTGTTGCCATAGAACATC
Hes1	TATTGCCAACTGGGAGCCTG	TCTAGCCCATTCATTCCTCT
Hes5	TCCAGAGCTCCAGGCATGGC	TCTATGCTGCTGTTGATGCG
Hey1	ACGAGACCATCGAGGTGGAA	TTCCTGGCCAAAACCTGGGA
Hey2	CCTTGTGAGGAAACGACCTC	CATCACTGAGCTTGTAGCGT

THE JOURNAL OF BIOLOGICAL CHEMISTRY VOL. 289, NO. 23, pp. 16430–16441, June 6, 2014
© 2014 by The American Society for Biochemistry and Molecular Biology, Inc. Published in the U.S.A.

HERC2 Targets the Iron Regulator FBXL5 for Degradation and Modulates Iron Metabolism

Received for publication, December 7, 2013, and in revised form, April 19, 2014 Published, JBC Papers in Press, April 28, 2014, DOI 10.1074/jbc.M113.541490

Toshiro Moroishi, Takayoshi Yamauchi, Masaaki Nishiyama, and Keiichi I. Nakayama[1]

From the Department of Molecular and Cellular Biology, Medical Institute of Bioregulation, Kyushu University, 3-1-1 Maidashi, Higashi-ku, Fukuoka, Fukuoka 812-8582, Japan

Background: FBXL5, the F-box protein subunit of an SCF-type ubiquitin-ligase complex, is a regulator of mammalian iron homeostasis.
Results: The HECT-type E3 ligase HERC2 binds to FBXL5 and regulates its stability.
Conclusion: HERC2 controls iron metabolism by promoting ubiquitin-dependent degradation of FBXL5.
Significance: Our results provide new mechanistic insight into the proteolytic control of iron metabolism.

FBXL5 (F-box and leucine-rich repeat protein 5) is the F-box protein subunit of, and therefore responsible for substrate recognition by, the SCF^{FBXL5} ubiquitin-ligase complex, which targets iron regulatory protein 2 (IRP2) for proteasomal degradation. IRP2 plays a central role in the maintenance of cellular iron homeostasis in mammals through posttranscriptional regulation of proteins that contribute to control of the intracellular iron concentration. The FBXL5-IRP2 axis is integral to control of iron metabolism *in vivo*, given that mice lacking FBXL5 die during early embryogenesis as a result of unrestrained IRP2 activity and oxidative stress attributable to excessive iron accumulation. Despite its pivotal role in the control of iron homeostasis, however, little is known of the upstream regulation of FBXL5 activity. We now show that FBXL5 undergoes constitutive ubiquitin-dependent degradation at the steady state. With the use of a proteomics approach to the discovery of proteins that regulate the stability of FBXL5, we identified the large HECT-type ubiquitin ligase HERC2 (HECT and RLD domain containing E3 ubiquitin protein ligase 2) as an FBXL5-associated protein. Inhibition of the HERC2-FBXL5 interaction or depletion of endogenous HERC2 by RNA interference resulted in the stabilization of FBXL5 and a consequent increase in its abundance. Such accumulation of FBXL5 in turn led to a decrease in the intracellular content of ferrous iron. Our results thus suggest that HERC2 regulates the basal turnover of FBXL5, and that this ubiquitin-dependent degradation pathway contributes to the control of mammalian iron metabolism.

Iron is an essential nutrient for almost all living organisms, with iron deficiency resulting in the impairment of various cellular processes including oxygen transport, energy production, and DNA repair (1). On the other hand, iron is highly reactive and can be deleterious to cells if present in excess (2). Given that both iron deficiency and iron overload are harmful to cells, cellular iron homeostasis is subject to strict regulation (3).

In mammalian cells, iron homeostasis is regulated through coordination of iron uptake, storage, export, and utilization (4). Coordinated expression of proteins mediating these processes is regulated at the posttranscriptional level by iron regulatory protein 1 (IRP1)[2] and IRP2. These two orthologous RNA-binding proteins interact with conserved cis-regulatory hairpin structures known as iron-responsive elements (IREs) during iron-limiting conditions to regulate the translation and stability of mRNAs for proteins that contribute to iron homeostasis (5). As a consequence of these interactions, IRP1 and IRP2 increase the size of the bioavailable (ferrous, Fe^{2+}) iron pool during iron-limiting conditions (6). When bioavailable iron levels are high, this activity of IRP1/2 is lost as a result of the assembly of a [4Fe-4S] cluster within IRP1 (holo-IRP1) or of the degradation of both apo-IRP1 (IRP1 without the [4Fe-4S] cluster) and IRP2 by the ubiquitin-proteasome system (7).

The stability of apo-IRP1 and IRP2 is dependent on the action of an iron- and oxygen-regulated SCF-type ubiquitin ligase, SCF^{FBXL5} (8, 9). FBXL5 (F-box and leucine-rich repeat protein 5) is a member of the F-box family of adaptor proteins that confer substrate specificity on SCF-type ubiquitin ligases (E3s), which consist of the RING-finger protein RBX1, the scaffold protein CUL1, and the adaptor protein SKP1 in addition to an F-box protein (10–12). Under iron-replete conditions, FBXL5 recruits apo-IRP1 and IRP2 to the SCF complex, resulting in their ubiquitylation. In contrast, under iron-limiting conditions, FBXL5 itself is targeted for ubiquitylation and degradation by the proteasome, resulting in the stabilization of apo-IRP1 and IRP2 and their interaction with IREs.

Indicative of the pivotal role of FBXL5 in the control of mammalian iron homeostasis, we have recently shown that mice lacking FBXL5 die early in embryogenesis as a result of deleterious effects of the accumulation of free iron (13). Additional ablation of IRP2, which dominates control of iron homeostasis *in vivo*, rescued this embryonic mortality of FBXL5-null mice, suggesting that strict regulation of IRP2 by FBXL5 is required for the maintenance of iron homeostasis as well as for viability during development. In addition, liver-specific ablation of FBXL5 was found to result in death from acute liver failure

[1] To whom correspondence should be addressed. Tel.: 81-92-642-6815; Fax: 81-92-642-6819; E-mail: nakayak1@bioreg.kyushu-u.ac.jp.

[2] The abbreviations used are: IRP, iron regulatory protein; IRE, iron-responsive element; FBXL5, F-box and leucine-rich repeat protein 5; SCF, SKP1–CUL1–F-box protein; HERC2, HECT and RLD domain containing E3 ubiquitin protein ligase 2; TetR, tetracycline repressor.

Downloaded from http://www.jbc.org/ at FUZOKU TOSHOKAN KYUSHU UNIV on November 17, 2014

when mice were fed a high-iron diet. The FBXL5-IRP2 axis is thus integral to control of iron metabolism *in vivo*. Despite recognition of its pivotal role in the regulation of iron homeostasis, however, little is known of the upstream mechanisms responsible for the control of FBXL5 activity.

A regulatory element that renders the stability of FBXL5 sensitive to iron resides within the hemerythrin-like domain at the NH_2 terminus of the protein (14). Hemerythrin is a member of a family of iron- and oxygen-binding proteins in bacteria and invertebrates. A previous study suggested that a degron present within the hemerythrin-like domain of FBXL5 becomes preferentially accessible to an as yet unknown E3 in the absence of iron binding to the domain, resulting in ubiquitin-dependent degradation of FBXL5 under iron-limiting conditions (15). The hemerythrin-like domain of FBXL5 is thus considered to be pivotal to the iron-dependent stability of the protein. It remains unclear how FBXL5 is regulated at the steady state, however.

We have now found that FBXL5 undergoes constitutive proteasomal degradation at the steady state, and that a mutant form of FBXL5 that lacks the hemerythrin-like domain is similarly degraded, suggesting the existence of a mechanism for regulation of FBXL5 stability that is independent of this domain. With the use of a proteomics approach, we identified the large HECT-type ubiquitin ligase HERC2 (HECT and RLD domain containing E3 ubiquitin protein ligase 2) as an FBXL5-interacting protein. Depletion of endogenous HERC2 by RNAi stabilized FBXL5 and thereby increased its abundance, resulting in dysregulation of its downstream targets. Our results indicate that HERC2 regulates the basal turnover of FBXL5 and thereby modulates iron metabolism.

EXPERIMENTAL PROCEDURES

Plasmids—Complementary DNAs encoding WT or mutant forms of human FBXL5; mouse SKP2, FBXW5, or FBXW7α; or fragments of human HERC2, each with an NH_2-terminal FLAG tag, were subcloned into pcDNA3 (Invitrogen). A cDNA encoding human ubiquitin, tagged at its NH_2 terminus with the HA epitope, was subcloned into pCGN (16).

Antibodies—Antibodies to FBXL5 (N0036) were obtained from NeoClone Biotechnology International, HERC2 (ab85832) were from Abcam, IRP1 (sc-14216) and IRP2 (sc-33682) were from Santa Cruz Biotechnology, transferrin receptor 1 (13-6800) from Invitrogen, SKP1 (610530) and HSP90 (610419) were from BD Biosciences, CUL1 (71-8700) was from Zymed Laboratories Inc., and the FLAG epitope (M2) was from Sigma.

Cell Culture and Transfection—HEK293T cells and HeLa cells were cultured under an atmosphere of 5% CO_2 at 37 °C in DMEM (Invitrogen) supplemented with 10% FBS (Invitrogen), 1 mM sodium pyruvate, penicillin (100 units/ml), streptomycin (100 mg/ml), 2 mM L-glutamine, and nonessential amino acids (10 μl/ml; Invitrogen). Transfection was performed with the FuGENE HD reagent (Roche Applied Science). The empty pcDNA3 plasmid was included to ensure that cells were transfected with equal amounts of total DNA.

Preparation of Lentiviral Vectors—Lentiviral vectors were prepared as described (17). Gene silencing by RNAi was performed with the lentivirus-based shRNA expression vector CSII-U6tet (18). The shRNA-encoding DNA oligonucleotide inserts were generated with the use of the Insert Design Tool for pSilencer vectors (Applied Biosystems). The target sequences were 5′-GGCCTTGCCTCCAGAAACA-3′ (HERC2-1) and 5′-GGAAAGCACTGGATTCGTT-3′ (HERC2-2) for HERC2 and 5′-GCATACAGCTCTGCAGTTTCC-3′ for FBXL5. An shRNA specific for LacZ (5′-AAGGCCAGACGCGAATTAT-3′), which did not match any existing sequence in the human database, was used as a control.

Tetracycline-inducible shRNA Expression System—HEK293T and HeLa cells were infected with a lentivirus encoding TetR (CSII-EF-TetR-IRES-puro) (18) for 2 days. The cells were then incubated with puromycin (5 μg/ml) for selection and amplification of puromycin-resistant cells. The TetR-expressing cells were then infected with lentiviruses encoding shRNAs. For induction of shRNA expression, the cells were incubated with doxycycline (1 μg/ml) for the indicated times, with replenishment of the drug after 48 h.

Immunoprecipitation and Immunoblot Analysis—HEK293T cells expressing FLAG-tagged proteins were lysed with a buffer comprising 50 mM Tris-HCl (pH 7.5), 150 mM NaCl, 0.5% Triton X-100, aprotinin (10 μg/ml), leupeptin (10 μg/ml), 1 mM PMSF, 400 μM Na_3VO_4, 400 μM EDTA, 10 mM NaF, and 10 mM sodium pyrophosphate. The lysates were centrifuged at 20,000 × *g* for 10 min at 4 °C to remove debris, and the resulting supernatants were adjusted with lysis buffer to achieve a protein concentration of 3 mg/ml. The supernatants were then incubated for 30 min at 4 °C with agarose beads conjugated with M2 antibodies to FLAG (Sigma). The resulting immunoprecipitates were washed three times with ice-cold lysis buffer, fractionated by SDS-PAGE, and subjected to immunoblot analysis with primary antibodies and HRP-conjugated secondary antibodies to mouse (Promega), rabbit (Promega), or goat (Santa Cruz Biotechnology) IgG. Immune complexes were detected with an ECL system (Thermo Scientific). For detection of the interaction between endogenous HERC2 and FBXL5, HEK293T cells were incubated for 4 h in the presence of the proteasome inhibitor MG132 (5 μM; Peptide Institute) and then subjected to extraction as described above. The resulting supernatants were subjected to immunoprecipitation for 1 h at 4 °C with antibodies to HERC2 (or control rabbit IgG) and protein A-Sepharose 4 Fast Flow (GE Healthcare). The immunoprecipitates were washed three times with lysis buffer and then subjected to immunoblot analysis, as described above.

Immunoaffinity Purification and Protein Identification by LC-MS/MS Analysis—A cDNA for FLAG-tagged FBXL5 was subcloned into pMX-puro-CMV (19). The resulting vector was introduced together with pCL-Ampho (Imgenex) into HEK293T cells with the use of FuGENE 6 (Promega). The recombinant retroviruses thereby generated were used to infect HEK293T cells, which were then subjected to selection in medium containing puromycin (5 μg/ml). The resulting cells (1×10^8) stably expressing FLAG-FBXL5 were incubated for 6 h in the presence of MG132 (10 μM) and then lysed in 8 ml of a lysis buffer containing 20 mM HEPES-NaOH (pH 7.5), 150 mM NaCl, 1% digitonin, 10 mM NaF, 10 mM $Na_4P_2O_7$, 0.4 mM Na_3VO_4, 0.4 mM EDTA, leupeptin (20 μg/ml), aprotinin (10 μg/ml), and 1 mM PMSF. The lysate was centrifuged at 20,000 × *g* for 20 min at 4 °C to remove debris, and the resulting

Downloaded from http://www.jbc.org/ at FUZUKU TOSHOKAN KYUSHU UNIV on November 11, 2014

supernatant was adjusted with lysis buffer to achieve a protein concentration of 3 mg/ml before incubation for 50 min at 4 °C with agarose beads conjugated with M2 antibodies to FLAG (Sigma). The beads were then washed three times with 4 ml of a solution containing 10 mM HEPES-NaOH (pH 7.5), 150 mM NaCl, and 0.1% Triton X-100, after which bead-bound proteins were eluted with 400 μl of FLAG peptide solution (500 μg/ml; Sigma), precipitated with ice-cold 20% TCA, and washed with acetone. The concentrated proteins were dissolved in SDS sample buffer, fractionated by SDS-PAGE on a 10.5% gel, and stained with silver. Individual lanes of the stained gel were sliced into 18 pieces, and proteins within these pieces were subjected to in-gel digestion with trypsin. The resulting peptides were subjected to LC-MS/MS analysis with an ion-trap mass spectrometer (LTQ-XL, Thermo Finnigan), and the obtained data sets were analyzed on the basis of spectral counting as described previously (19).

RT and Real-time PCR Analysis—Total RNA (1 μg) isolated from cells with the use of Isogen (Nippon Gene) was subjected to RT and real-time PCR analysis with primers (forward and reverse, respectively) specific for human FBXL5 (5′-GCCTATGGAATCATGCTGAAGAGC-3′ and 5′-GCATTACCTCAGGAGGAAGATGGG-3′) and human GAPDH (5′-GCAAATTCCATGGCACCGT-3′ and 5′-TCGCCCCACTTGATTTTGG-3′), as described previously (20). The amount of FBXL5 mRNA was normalized by the corresponding amount of GAPDH mRNA.

Determination of Ferrous Iron—The concentration of Fe^{2+} was determined with the phenanthroline method as described previously (21), with slight modifications. In brief, shRNA-expressing HEK293T cells (1×10^8) were harvested with trypsin, washed five times with 1 ml of PBS (Invitrogen), and subjected to ultrasonic treatment in 500 μl of a solution (pH 4.6) containing 500 μM 1,10-phenanthroline (Sigma) and 100 mM sodium acetate (Sigma). The samples were then centrifuged at 100,000 × *g* for 30 min at 4 °C, and the absorbance of the resulting supernatants was measured immediately at 510 nm for the spectrophotometric detection of Fe^{2+}. A certified iron standard ($FeSO_4$; Sigma) was used to determine Fe^{2+} levels. A standard curve for Fe^{2+} concentrations between 0.2 and 2 μg/ml revealed a linearity of response with a slope of ~1. Samples were diluted appropriately to fall within the linear range. Cellular Fe^{2+} content was expressed as a percentage for control cells.

RESULTS

FBXL5 Undergoes Proteasomal Degradation in a Manner Independent of Its Hemerythrin-like Domain—To explore the mechanisms by which the cellular abundance of FBXL5 is controlled, we examined the stability of FBXL5 at steady state in HEK293T cells cultured in the presence of the protein synthesis inhibitor cycloheximide and in the absence or presence of the proteasome inhibitor MG132. FBXL5 was rapidly degraded, with a half-life of <1 h, in the absence of MG132, whereas this rapid turnover was almost completely blocked by the proteasome inhibitor (Fig. 1*A*). These results suggested that FBXL5 is constitutively degraded and that this basal degradation is dependent largely on the proteasome.

Consistent with previous observations suggesting that FBXL5 is targeted for proteasomal degradation in an iron-dependent manner (14), we found that the level of FBXL5 was greatly diminished when iron was limiting and markedly increased under iron-replete conditions (Fig. 1*B*). A fragment of FBXL5 comprising residues 1–161 also showed similar iron-dependent changes in stability, whereas an FBXL5 mutant lacking this region did not (Fig. 1*C*), suggesting that a regulatory element that renders FBXL5 stability sensitive to iron resides within its hemerythrin-like domain (amino acids 1–161). To investigate the requirement for the hemerythrin-like domain in the basal degradation of FBXL5, we measured the stability of the FBXL5(Δ1–161) mutant in HEK293T cells cultured in the presence of cycloheximide and in the absence or presence of MG132. As with the WT protein, FBXL5(Δ1–161) was rapidly degraded, with a half-life of <1 h, in the absence of MG132, whereas this rapid turnover was markedly attenuated by the proteasome inhibitor (Fig. 1*D*). These results suggested that an FBXL5 mutant that lacks the hemerythrin-like domain still undergoes proteasome-dependent degradation at the steady state, and that this domain is therefore dispensable for the basal degradation of FBXL5.

Identification of HERC2 as an FBXL5-associated Protein by a Proteomics Approach—To elucidate the mechanism underlying the basal turnover of FBXL5, we adopted a proteomics approach to identify molecules that associate with this protein. Lysates of HEK293T cells stably infected with a retroviral expression vector for FLAG epitope-tagged FBXL5 were subjected to immunoprecipitation with antibodies to FLAG, and the resulting immunoprecipitated proteins were eluted from the antibody-coated beads with the FLAG peptide and subjected to SDS-PAGE followed by silver staining (Fig. 2*A*). LC-MS/MS analysis of peptides derived from the fractionated proteins identified CUL1 and SKP1 (both of which are components of the SCF^{FBXL5} E3 complex) as well as IRP1 and IRP2, both of which were previously identified as substrates for FBXL5 (Fig. 2*B*) (8, 9). These results thus validated our approach and revealed its high reproducibility. Among the other identified FBXL5-interacting proteins, we focused on HERC2, given that it possesses a COOH-terminal HECT domain, a hallmark of a subfamily of E3 ligases (22).

To confirm the interaction between FBXL5 and HERC2 in mammalian cells, we transfected HEK293T cells with expression vectors for FLAG-tagged F-box proteins including SKP2, FBXL5, FBXW5, and FBXW7α and subjected cell lysates to immunoprecipitation with antibodies to FLAG. Immunoblot analysis of the resulting precipitates with antibodies to HERC2 revealed that endogenous HERC2 interacted with FLAG-FBXL5, but not with FLAG-SKP2, FLAG-FBXW5, or FLAG-FBXW7α (Fig. 2*C*). To determine whether formation of an SCF complex by FBXL5 is required for its association with HERC2, we replaced two amino acids (Pro^{209} and Glu^{211}) in the F-box domain of FBXL5 that are essential for its binding to CUL1 with alanine (19). This FBXL5(PE/AA) mutant failed to bind endogenous CUL1 but retained the ability to associate with endogenous HERC2 (Fig. 2*C*). These results thus suggested that FLAG-FBXL5 interacts specifically with endogenous HERC2 in a manner independent of SCF complex formation.

Downloaded from http://www.jbc.org/ at FUZOKU TOSHOKAN KYUSHU UNIV on November 17, 2014

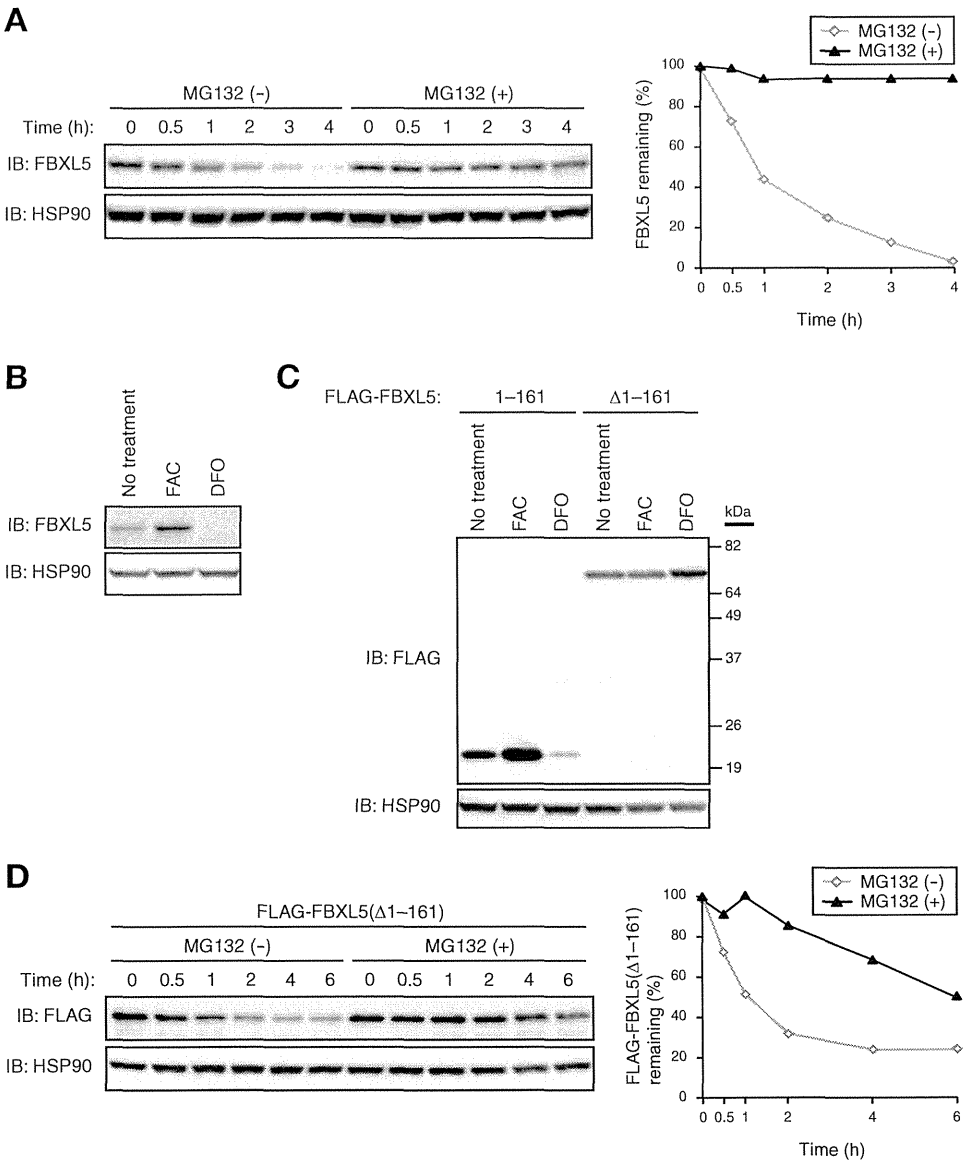

FIGURE 1. **FBXL5 undergoes constitutive proteasomal degradation in a manner independent of its hemerythrin-like domain.** *A*, HEK293T cells incubated with cycloheximide (100 μg/ml) for the indicated times in the absence or presence of the proteasome inhibitor MG132 (10 μM) were subjected to immunoblot (*IB*) analysis with antibodies to FBXL5 and HSP90 (loading control). The percentage of FBXL5 remaining after the various incubation times was quantitated by image analysis. *B*, HEK293T cells incubated for 16 h in the absence or presence of ferric ammonium citrate (*FAC*; 100 μg/ml) or the ferric-iron chelator desferrioxamine (*DFO*; 100 μM) were subjected to immunoblot analysis with antibodies to FBXL5 and HSP90. *C*, HEK293T cells transfected with expression vectors for FLAG-FBXL5(1–161) or FLAG-FBXL5(Δ1–161) were incubated for 6 h in the absence or presence of FAC (100 μg/ml) or DFO (100 μM) and then subjected to immunoblot analysis with antibodies to FLAG and to HSP90. *D*, HEK293T cells transfected with an expression vector for FLAG-FBXL5(Δ1–161) were exposed to cycloheximide (100 μg/ml) for the indicated times in the absence or presence of MG132 (10 μM) and then subjected to immunoblot analysis with antibodies to FLAG and HSP90. The percentage of FLAG-FBXL5(Δ1–161) remaining after the various incubation times was quantitated by image analysis.

We also performed similar experiments to detect the interaction between endogenous proteins. Immunoprecipitates prepared from HEK293T cell extracts with antibodies to HERC2 were subjected to immunoblot analysis with antibodies to FBXL5. Endogenous FBXL5 was co-immunoprecipitated with endogenous HERC2 (Fig. 2*D*), suggesting that HERC2 interacts with FBXL5 under physiological conditions.

Molecular Dissection of the HERC2-FBXL5 Interaction—We next investigated which region of FBXL5 is required for binding to HERC2 by generating a series of FLAG-tagged deletion mutants of FBXL5 (Fig. 3*A*) and examining their ability to associate with endogenous HERC2 with a co-immunoprecipitation assay in HEK293T cells. Whereas full-length FBXL5 and all three mutants that contained amino acids 257–297 interacted with HERC2, all the other mutants that lacked this region failed to do so (Fig. 3, *B* and *C*), suggesting that residues 257–297 are required for the interaction of FBXL5 with HERC2. Given that this region of FBXL5 is adjacent to the F-box domain, we examined the association of FBXL5(Δ257–297) with CUL1 and SKP1. This mutant retained the ability to interact with both CUL1 and SKP1 (Fig. 3*C*). On the other hand, an FBXL5 mutant lacking the F-box domain (Δ195–256) was found to bind to HERC2 but not to CUL1 or SKP1. Furthermore, full-length FBXL5 was found to associate with both CUL1-SKP1 and HERC2, con-

Downloaded from http://www.jbc.org/ at ASBMB on June 17, 2014

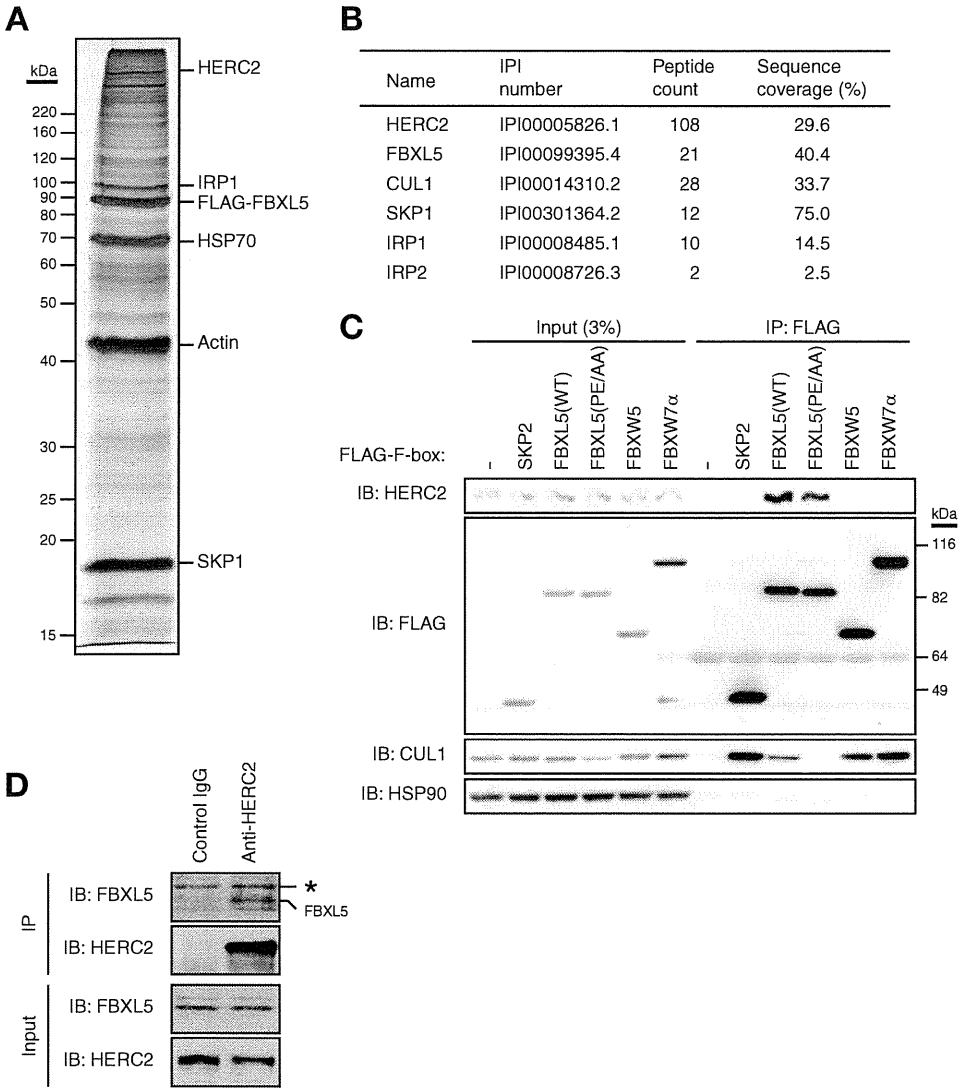

Name	IPI number	Peptide count	Sequence coverage (%)
HERC2	IPI00005826.1	108	29.6
FBXL5	IPI00099395.4	21	40.4
CUL1	IPI00014310.2	28	33.7
SKP1	IPI00301364.2	12	75.0
IRP1	IPI00008485.1	10	14.5
IRP2	IPI00008726.3	2	2.5

FIGURE 2. **Identification of HERC2 as a protein that interacts with FBXL5.** *A*, HEK293T cells stably expressing FLAG-tagged FBXL5 were incubated for 6 h in the presence of MG132 (10 μM) and then subjected to immunoaffinity purification with agarose-conjugated antibodies to FLAG. The purified proteins were fractionated by SDS-PAGE and stained with silver. The positions of bands corresponding to various purified proteins are indicated. *B*, the proteins found to interact with FLAG-FBXL5 in *A* were identified by LC-MS/MS analysis. For clarity, only HERC2 and previously identified FBXL5-interacting proteins are listed. The peptide count as well as the percentage sequence coverage for each protein are also shown. *C*, HEK293T cells transfected (or not) with expression vectors for FLAG-SKP2, FLAG-tagged WT, or mutant (PE/AA) forms of FBXL5, FLAG-FBXW5, or FLAG-FBXW7α were subjected to immunoprecipitation (*IP*) with antibodies to FLAG, and the resulting precipitates as well as a portion of the original cell lysates (*Input*) were subjected to immunoblot (*IB*) analysis with antibodies to the indicated proteins. *D*, HEK293T cells were incubated for 4 h in the presence of MG132 (5 μM) and then subjected to immunoprecipitation with antibodies to HERC2 (or with normal control IgG), and the resulting precipitates as well as a portion of the original cell lysates (*Input*) were subjected to immunoblot analysis with antibodies to FBXL5 and HERC2. The *asterisk* indicates a nonspecific band.

sistent with our observation that FBXL5 interacts with HERC2 in a manner independent of the SCF complex formation.

We also determined the region of HERC2 required for binding to FBXL5. Various fragments of HERC2 fused with the FLAG epitope were tested for the ability to interact with endogenous FBXL5 with a co-immunoprecipitation assay in HEK293T cells (Fig. 4). Whereas both fragments that contained amino acids 2930–3327 (a region that includes the RCC1–2 domain) interacted with FBXL5, all the other mutants that lacked this region failed to do so, suggesting that residues 2930–3327 are sufficient for the interaction of HERC2 with FBXL5. Our observations thus indicated that a region of HERC2 that includes the RCC1–2 domain (amino acids 2930–3327) interacts with a region adjacent to the F-box domain of FBXL5 (amino acids 257–297).

HERC2 Mediates Ubiquitin-dependent Degradation of FBXL5—Given that HERC2 contains a HECT domain, a hallmark of a subfamily of E3 ubiquitin ligases, we hypothesized that interaction of HERC2 with FBXL5 results in the ubiquitin-dependent proteolysis of the latter protein. To test this possibility, we first transfected HEK293T cells with various amounts of an expression vector for the FBXL5 binding domain of HERC2 (amino acids 2930–3327), which would be expected to inhibit the interaction between endogenous HERC2 and FBXL5. Immunoblot analysis with antibodies to FBXL5 revealed that expression of FLAG-HERC2(2930–3327) in HEK293T cells increased the abundance of endogenous FBXL5 in a concentration-dependent manner (Fig. 5*A*). We next measured the stability of an FBXL5 mutant that lacks the HERC2 binding domain (amino acids 257–297). Cycloheximide chase

Downloaded from http://www.jbc.org/ at FUZOKU TOSHOKAN KYUSHU UNIV on November 17, 2014

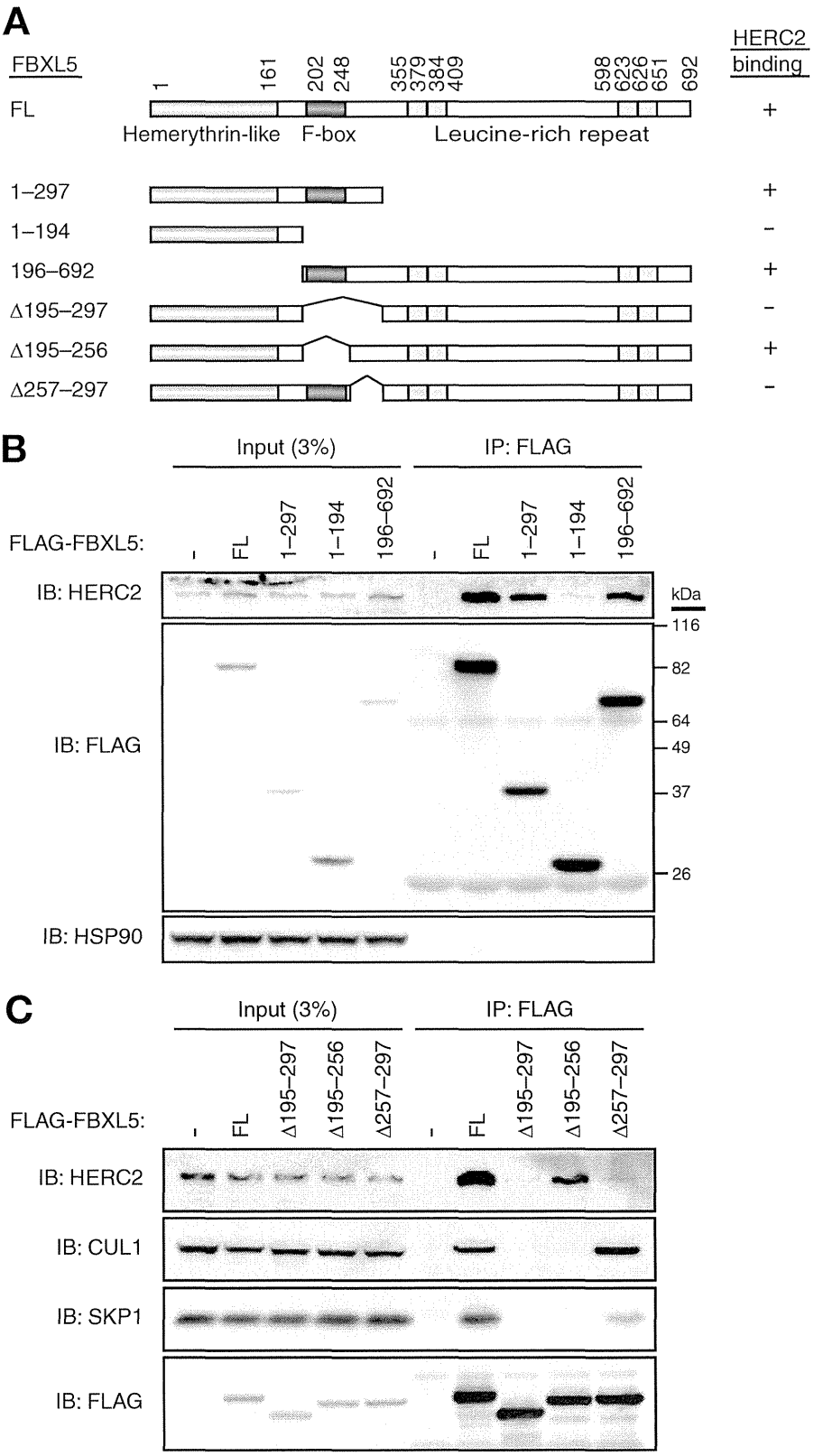

FIGURE 3. **Delineation of the region of FBXL5 responsible for the interaction with HERC2.** *A*, domain organization of full-length (*FL*) human FBXL5 and structure of deletion mutants thereof. A summary of the ability of the mutants to bind HERC2 as determined in *B* and *C* is shown on the *right*. *B* and *C*, HEK293T cells transfected (or not) with expression vectors for FLAG-tagged full-length or mutant forms of FBXL5 were subjected to immunoprecipitation with antibodies to FLAG, and the resulting precipitates as well as a portion of the original cell lysates were subjected to immunoblot (*IB*) analysis with antibodies to the indicated proteins.

Downloaded from http://www.jbc.org/ at UNIVERSITY OF CALIFORNIA SAN DIEGO on November 17, 2014

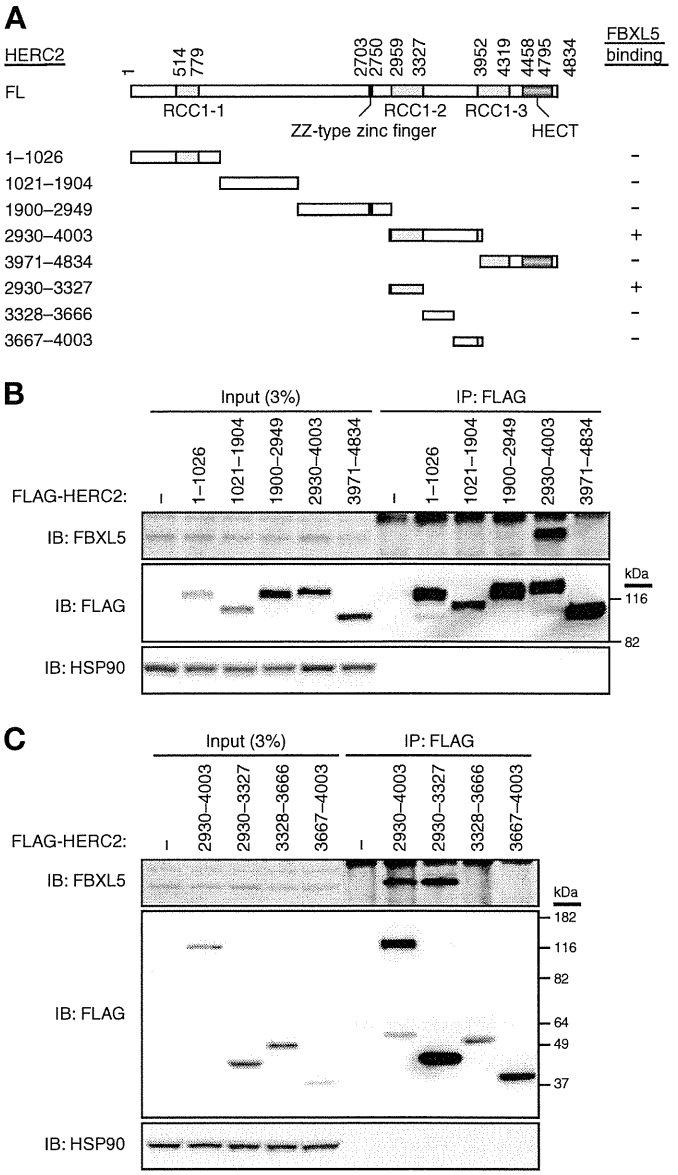

FIGURE 4. **Delineation of the region of HERC2 responsible for the interaction with FBXL5.** *A*, domain organization of human HERC2 and structure of deletion mutants thereof. A summary of the ability of the mutants to bind FBXL5 as determined in *B* and *C* is shown on the *right*. *B* and *C*, HEK293T cells transfected (or not) with expression vectors for FLAG-tagged mutants of HERC2 were subjected to immunoprecipitation with antibodies to FLAG, and the resulting precipitates as well as a portion of the original cell lysates were subjected to immunoblot (*IB*) analysis with antibodies to the indicated proteins.

analysis revealed that half-life of the FBXL5(Δ257–297) mutant in HEK293T cells was substantially longer than that of the WT protein (Fig. 5*B*). These results suggested that HERC2 binding destabilizes FBXL5 at the steady state. To investigate further the mechanism of basal FBXL5 degradation, we measured the stability of the FBXL5(PE/AA) mutant (which does not assemble into an SCF complex), given that the F-box subunits of SCF E3 complexes are often subjected to autoubiquitylation and degradation (23). The half-life of FBXL5(PE/AA) did not differ from that of WT FBXL5 (Fig. 5*B*), suggesting that the basal turnover of FBXL5 is regulated in a manner independent of its assembly into an SCF complex. Collectively, our observations suggested that the stability of FBXL5 is regulated by HERC2, but not through autoubiquitylation resulting from formation of the SCF^{FBXL5} complex.

To confirm that HERC2 indeed regulates the stability of FBXL5, we examined the effect of shRNA-mediated depletion of endogenous HERC2 on the steady state level of endogenous FBXL5. Depletion of HERC2 in HEK293T cells resulted in the accumulation of FBXL5 in proportion to the extent of depletion (Fig. 6*A*), without a corresponding effect on the amount of FBXL5 mRNA (Fig. 6*B*). These results suggested that endogenous HERC2 regulates the abundance of FBXL5 at a posttranscriptional level.

For reproducible expression of shRNA, we took advantage of HEK293T cells in which a tetracycline-inducible construct encoding HERC2 shRNA was stably integrated. Immunoblot analysis revealed a substantial decrease in the abundance of HERC2 in such cells as early as 48 h after the onset of doxycycline treatment (Fig. 6*C*). We therefore cultured these cells with doxycycline for 48 h to deplete HERC2 and then subjected the cells to cycloheximide chase analysis to measure the stability of FBXL5 (Fig. 6*D*). The half-life of FBXL5 was markedly increased in cells depleted of HERC2 compared with that in control cells. Furthermore, to evaluate the effect of HERC2 depletion on the ubiquitylation of FBXL5, we transfected HERC2-depleted HEK293T cells with expression vectors for HA-tagged ubiquitin and FLAG-tagged WT or mutant (PE/AA) forms of FBXL5 and then subjected lysates of the transfected cells to immunoprecipitation with antibodies to FLAG. Immunoblot analysis of the resulting precipitates revealed that depletion of endogenous HERC2 resulted in a marked decrease in the ubiquitylation levels of both FLAG-FBXL5(WT) and FLAG-FBXL5(PE/AA) (Fig. 6*E*). The extent of ubiquitylation of FLAG-FBXL5(PE/AA) did not differ from that of FLAG-FBXL5(WT) in control cells, suggesting that basal ubiquitylation of FBXL5 is mediated in a manner independent of its assembly into an SCF complex, again arguing against an autoubiquitylation model for control of basal FBXL5 degradation. Collectively, our observations suggested that HERC2 serves as an E3 ligase for FBXL5 and promotes its basal turnover.

We also examined the stability of FBXL5 in the absence or presence of HERC2 in HeLa cells. As observed with HEK293T cells, the half-life of FBXL5 was markedly greater in HERC2-depleted HeLa cells than in the corresponding control cells (Fig. 6*F*), suggesting that the role of HERC2 in regulation of the basal turnover of FBXL5 is not specific to one cell line.

HERC2 Modulates Iron Metabolism by Regulating the Basal Turnover of FBXL5—Given that HERC2 was shown to serve as an E3 ligase for FBXL5 at the steady state, we next examined whether HERC2 also mediates iron-dependent changes in FBXL5 stability. We cultured control or HERC2-depleted HEK293T cells under iron-replete conditions and then subjected them to iron limitation for various times before immunoblot analysis (Fig. 7*A*). Although HERC2 depletion resulted in a marked increase in the abundance of FBXL5 before iron chelation, the subsequent rate of degradation of FBXL5 in cells depleted of HERC2 was almost identical to that in control cells, suggesting that HERC2 is dispensable for iron-dependent changes in the stability of FBXL5. Our observations thus indi-

Downloaded from http://www.jbc.org/ at FUZOKU TOSHOKAN KYUSHU UNIV on November 17, 2014

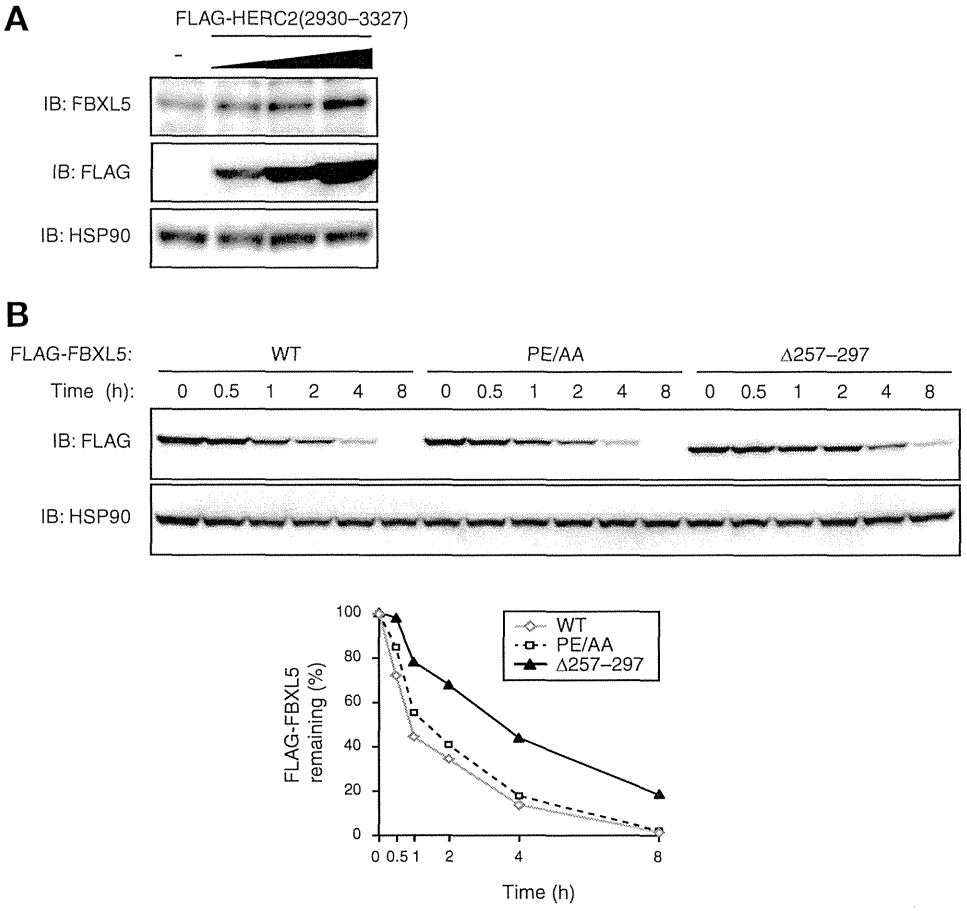

FIGURE 5. **Inhibition of HERC2-FBXL5 interaction stabilizes FBXL5.** *A*, HEK293T cells transfected (or not) with various amounts (1×, 2×, 4×) of an expression vector for FLAG-HERC2(2930–3327) were subjected to immunoblot analysis with antibodies to the indicated proteins. *B*, HEK293T cells transfected with expression vectors for FLAG-FBXL5(WT), FLAG-FBXL5(PE/AA), or FLAG-FBXL5(Δ257–297) were exposed to cycloheximide (100 μg/ml) for the indicated times and then subjected to immunoblot analysis with antibodies to FLAG and HSP90. The percentage of the FLAG-tagged proteins remaining after the various incubation times was quantitated by image analysis.

cated that HERC2 regulates the basal turnover of FBXL5 rather than its iron-dependent degradation.

To evaluate the role of HERC2 in regulation of intracellular iron homeostasis, we examined the effects of HERC2 depletion on the expression of proteins related to such homeostasis (Fig. 7*B*). For both HEK293T and HeLa cells, the increase in the abundance of FBXL5 in cells depleted of HERC2 was associated with a decrease in the amounts of IRP1 and IRP2, which in turn was accompanied by a small but reproducible decrease in the abundance of transferrin receptor 1, the mRNA that is stabilized by IRP1/2 binding (24). On the other hand, the response of these various iron homeostasis-related proteins to changes in iron availability was maintained in the HERC2-depleted cells (Fig. 7*C*), consistent with the finding that HERC2 is dispensable for iron-dependent degradation of FBXL5. Furthermore, the additional depletion of FBXL5 greatly attenuated the effects of HERC2 depletion (Fig. 7*C*), suggesting that the latter effects are mediated by up-regulation of FBXL5 expression. Our results thus indicated that the accumulation of FBXL5 in HERC2-depleted HEK293T and HeLa cells results in dysregulation of the expression of proteins related to iron homeostasis.

Finally, we examined how such FBXL5 accumulation resulting from HERC2 depletion affects cellular iron homeostasis. The level of ferrous iron (Fe^{2+}) in HERC2-depleted HEK293T cells was significantly lower than that in control cells (Fig. 7*D*), suggesting that accumulated FBXL5 prevented Fe^{2+} loading, likely as a result of reduced IRP1/2 expression, in the former cells. We confirmed that additional depletion of FBXL5 greatly attenuated this effect of HERC2 depletion, suggesting that the effect is indeed mediated by up-regulation of FBXL5 expression (Fig. 7*D*). Collectively, our observations thus indicated that HERC2 modulates iron metabolism by regulating the amount of FBXL5.

DISCUSSION

Iron homeostasis in mammals is strictly controlled to ensure provision of a proper amount of iron to cells. Regulation of IRP1/2 stability by the ubiquitin-proteasome pathway is critical for cells to maintain an appropriate ferrous iron (Fe^{2+}) content, and thereby to avoid deleterious iron deficiency and prevent iron excess (25). FBXL5 plays a pivotal role in the control of iron metabolism by promoting the ubiquitin-dependent degradation of IRP1/2 under iron-replete conditions (13). Furthermore, a decline in cellular iron availability and consequent loss of direct iron binding to the hemerythrin-like domain of FBXL5 results in the ubiquitylation of FBXL5 itself by an as yet unknown E3 followed by its degradation (8, 9).

Downloaded from http://www.jbc.org/ at FUZOKU TOSHOKAN KYUSHU UNIV on November 17, 2014

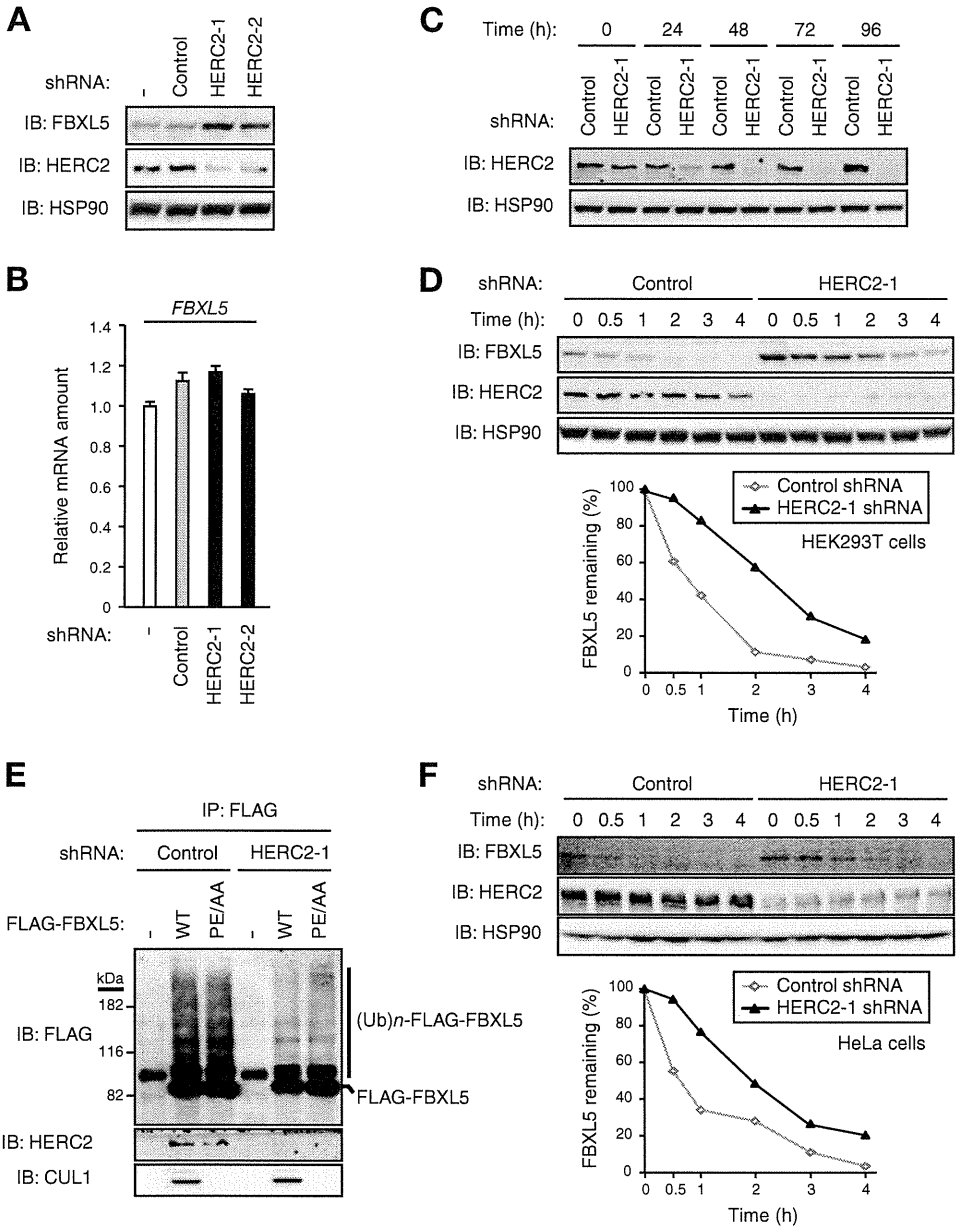

FIGURE 6. **Depletion of endogenous HERC2 stabilizes FBXL5.** *A*, HEK293T cells infected (or not) with lentiviral vectors encoding shRNAs specific for LacZ (control) or HERC2 (HERC2–1 or HERC2–2) for 48 h were subjected to immunoblot analysis with antibodies to the indicated proteins. *B*, total RNA extracted from cells infected as in *A* was subjected to RT and real-time PCR analysis of FBXL5 mRNA. Data are mean ± S.D. of triplicates from a representative experiment. *C*, tetracycline repressor (*TetR*)-expressing HEK293T cells were infected with lentiviral vectors encoding shRNAs specific for LacZ (control) or HERC2, incubated with doxycycline (1 μg/ml) for the indicated times, and then subjected to immunoblot (*IB*) analysis with antibodies to the indicated proteins. *D*, HEK293T cells infected as in *C* were incubated with doxycycline for 48 h and then exposed to cycloheximide (100 μg/ml) for the indicated times before immunoblot analysis with antibodies to the indicated proteins. The percentage of FBXL5 remaining after the various incubation times was quantitated by image analysis. *E*, HEK293T cells infected and treated with doxycycline as in *D* were transfected with expression vectors for HA-ubiquitin and for either FLAG-FBXL5(WT) or FLAG-FBXL5(PE/AA). The cells were then incubated for 4 h in the presence of MG132 (10 μM) prior to immunoprecipitation with antibodies to FLAG. The resulting precipitates were subjected to immunoblot analysis with antibodies to the indicated proteins. The positions of bands corresponding to polyubiquitylated ($(Ub)_n$) forms of FLAG-FBXL5 proteins are indicated. *F*, TetR-expressing HeLa cells were infected with lentiviral vectors encoding shRNAs specific for LacZ (control) or HERC2, incubated with doxycycline for 48 h, and then exposed to cycloheximide for the indicated times before immunoblot analysis with antibodies to the indicated proteins. The percentage of FBXL5 remaining after the various incubation times was quantitated by image analysis.

Recent molecular approaches have provided insight into the iron-dependent regulation of FBXL5 stability. The hemerythrin-like domain at the NH_2 terminus of FBXL5 is essential and sufficient for iron sensitivity of stability (14). Mutation of the iron-ligating residues in this domain results in constitutive destabilization of FBXL5, suggesting that iron binding is essential for protein stabilization. Moreover, residues 77–81 within the hemerythrin-like domain appear to constitute part of a degron responsible for iron-dependent degradation of FBXL5 (15). These observations thus suggest a model in which the hemerythrin-like domain acts as an iron-binding switch that regulates accessibility of the degron to an as yet unknown E3.

We now propose an additional mechanism for ubiquitin-dependent regulation of FBXL5 stability, providing further evidence for the prominent role of the ubiquitin-proteasome sys-

Downloaded from http://www.jbc.org/ at FUZOKU TOSHOKAN KYUSHU UNIV on November 17, 2014

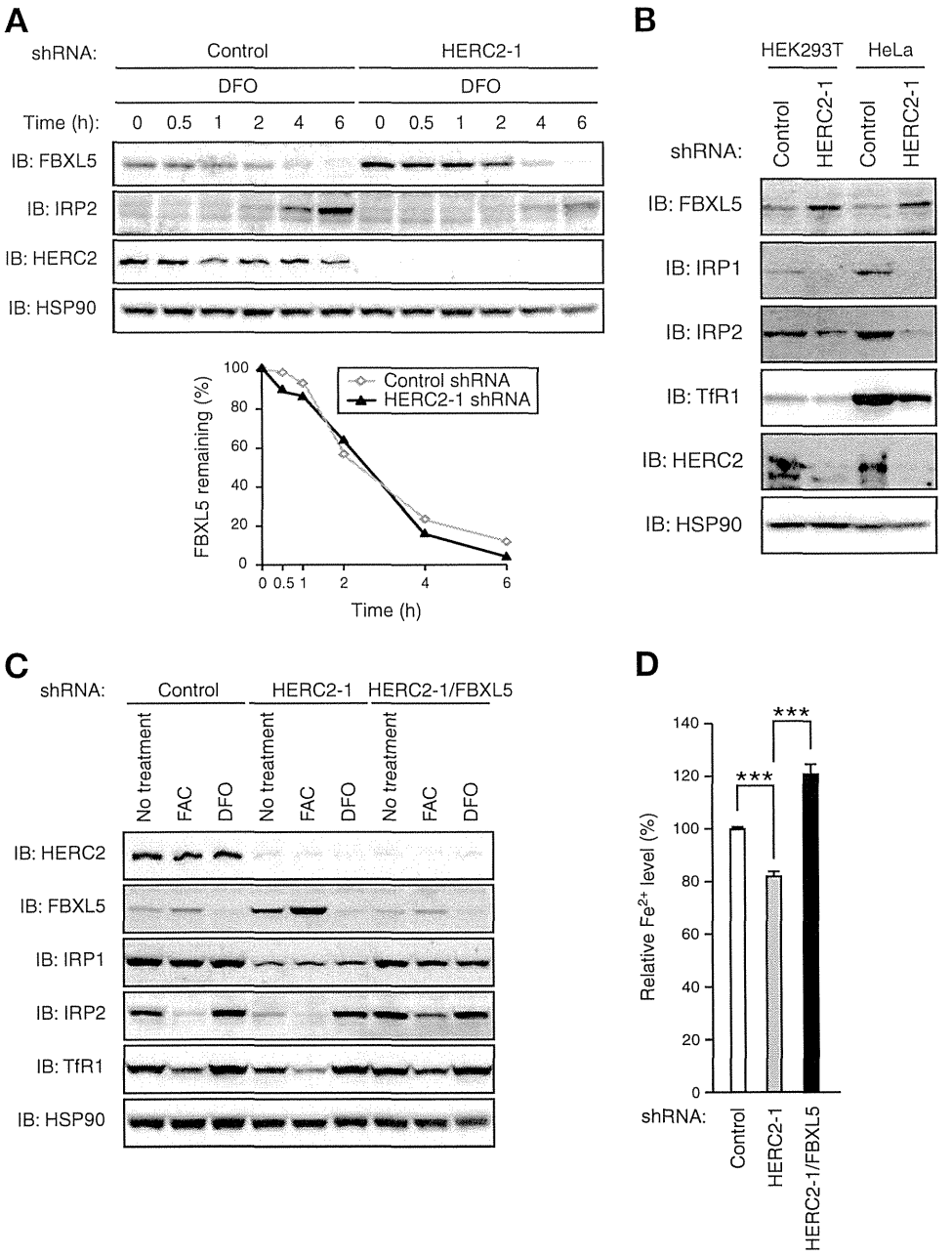

FIGURE 7. **HERC2 controls iron metabolism by regulating the basal degradation of FBXL5.** *A*, TetR-expressing HEK293T cells were infected with lentiviral vectors encoding LacZ (*control*) or HERC2 shRNAs, treated with doxycycline (1 μg/ml) for 48 h, incubated with ferric ammonium citrate (*FAC*) (100 μg/ml) for 16 h, and then exposed to desferrioxamine (*DFO*) (100 μM) for the indicated times before immunoblot (*IB*) analysis with antibodies to the indicated proteins. The percentage of FBXL5 remaining after the various incubation times was quantitated by image analysis. *B*, TetR-expressing HEK293T or HeLa cells infected with lentiviral vectors encoding LacZ (control) or HERC2 shRNAs were treated with doxycycline for 48 h and then subjected to immunoblot analysis with antibodies to the indicated proteins. *C*, TetR-expressing HEK293T cells infected with lentiviral vectors encoding LacZ (control), HERC2, or FBXL5 shRNAs, as indicated, were treated with doxycycline for 48 h, incubated in the absence or presence of FAC (100 μg/ml) or DFO (100 μM) for an additional 12 h, and then subjected to immunoblot analysis with antibodies to the indicated proteins. *D*, ferrous iron content of HEK293T cells infected and treated with doxycycline as in *C*. Data are mean ± S.D. from three independent experiments. ***, $p < 0.005$ (two-tailed Student's *t* test).

tem in the control of iron homeostasis. We have shown that FBXL5 is constitutively degraded at the steady state in a manner independent of its hemerythrin-like domain. Our biochemical results suggest that the large HECT-type ubiquitin ligase HERC2 is responsible for the basal degradation of FBXL5. HERC2 interacts with a region of FBXL5 immediately downstream of the F-box domain, and it regulates the basal turnover of FBXL5 rather than its iron-dependent degradation. Our findings further indicate that HERC2 sets the steady state level of FBXL5 and thereby modulates iron metabolism.

The human *HERC2* gene comprises 93 exons and encodes a 4834-amino acid protein with a predicted molecular size of 528 kDa (26). It is a highly mutable gene located at a deletion breakpoint hot spot on human chromosome 15q11-q13 (27). A homozygous missense mutation of *HERC2* is associated with a global developmental delay and autism spectrum disorder (28).

Downloaded from http://www.jbc.org/ at NOSHIRO TOKUDA on June 11, 2014

Although the function of HERC2 had long remained unknown, the protein was recently shown to contribute to the response of cells to DNA damage. HERC2 is thus recruited to sites of DNA double strand breaks and facilitates assembly of the ubiquitin-conjugating enzyme UBC13 with RNF8 (RING finger protein 8), thereby promoting ubiquitin-dependent retention of repair factors (29). HERC2 also shuttles between the nucleus and the cytoplasm, acting as an E3 ubiquitin ligase that targets xeroderma pigmentosum A in the circadian control of nucleotide excision repair (30) as well as BRCA1 (breast cancer 1) in control of the cell cycle (31). These observations suggest that HERC2 might regulate multiple aspects of the DNA damage response by contributing to the ubiquitylation and degradation of key protein participants (32).

DNA repair proteins commonly require iron as a cofactor (33), with this requirement likely endowing iron with protective effects against DNA damage (34). We have now uncovered a function of HERC2 that relates to iron metabolism. Cells exposed to DNA damage might require iron to facilitate the production of DNA repair proteins. In this regard, it is of interest that HERC2 also sets the cellular iron concentration by regulating the abundance of FBXL5.

Collectively, our observations suggest the existence of at least two distinct pathways for the ubiquitin-dependent regulation of FBXL5 stability, with these two pathways being responsible for the basal degradation and the iron-dependent degradation of the protein. These pathways might contribute differentially to FBXL5 degradation in a context-dependent manner. Further molecular analysis of the regulation of FBXL5, including identification of the as yet unknown E3 for the iron-dependent degradation pathway, should provide new insight into the control of iron metabolism mediated by ubiquitin-dependent proteolysis.

Acknowledgments—We thank H. Miyoshi and S. Yonehara for lentiviral vectors, T. Kitamura for pMX-puro, M. Oda and E. Koba for technical assistance, and T. Asano for discussion.

REFERENCES

1. Andrews, N. C., and Schmidt, P. J. (2007) Iron homeostasis. *Annu. Rev. Physiol.* **69,** 69–85
2. Prohaska, R., Sibon, O. C., Rudnicki, D. D., Danek, A., Hayflick, S. J., Verhaag, E. M., Vonk, J. J., Margolis, R. L., and Walker, R. H. (2012) Brain, blood, and iron: perspectives on the roles of erythrocytes and iron in neurodegeneration. *Neurobiol. Dis.* **46,** 607–624
3. De Domenico, I., McVey Ward, D., and Kaplan, J. (2008) Regulation of iron acquisition and storage: consequences for iron-linked disorders. *Nat. Rev. Mol. Cell Biol.* **9,** 72–81
4. Hentze, M. W., Muckenthaler, M. U., Galy, B., and Camaschella, C. (2010) Two to tango: regulation of mammalian iron metabolism. *Cell* **142,** 24–38
5. Rouault, T. A. (2006) The role of iron regulatory proteins in mammalian iron homeostasis and disease. *Nat. Chem. Biol.* **2,** 406–414
6. Wang, J., and Pantopoulos, K. (2011) Regulation of cellular iron metabolism. *Biochem. J.* **434,** 365–381
7. Evstatiev, R., and Gasche, C. (2012) Iron sensing and signalling. *Gut* **61,** 933–952
8. Salahudeen, A. A., Thompson, J. W., Ruiz, J. C., Ma, H. W., Kinch, L. N., Li, Q., Grishin, N. V., and Bruick, R. K. (2009) An E3 ligase possessing an iron-responsive hemerythrin domain is a regulator of iron homeostasis. *Science* **326,** 722–726
9. Vashisht, A. A., Zumbrennen, K. B., Huang, X., Powers, D. N., Durazo, A., Sun, D., Bhaskaran, N., Persson, A., Uhlen, M., Sangfelt, O., Spruck, C., Leibold, E. A., and Wohlschlegel, J. A. (2009) Control of iron homeostasis by an iron-regulated ubiquitin ligase. *Science* **326,** 718–721
10. Jin, J., Cardozo, T., Lovering, R. C., Elledge, S. J., Pagano, M., and Harper, J. W. (2004) Systematic analysis and nomenclature of mammalian F-box proteins. *Genes Dev.* **18,** 2573–2580
11. Nakayama, K. I., and Nakayama, K. (2006) Ubiquitin ligases: cell-cycle control and cancer. *Nat. Rev. Cancer* **6,** 369–381
12. Skaar, J. R., Pagan, J. K., and Pagano, M. (2013) Mechanisms and function of substrate recruitment by F-box proteins. *Nat. Rev. Mol. Cell. Biol.* **14,** 369–381
13. Moroishi, T., Nishiyama, M., Takeda, Y., Iwai, K., and Nakayama, K. I. (2011) The FBXL5-IRP2 axis is integral to control of iron metabolism *in vivo*. *Cell Metab.* **14,** 339–351
14. Chollangi, S., Thompson, J. W., Ruiz, J. C., Gardner, K. H., and Bruick, R. K. (2012) Hemerythrin-like domain within F-box and leucine-rich repeat protein 5 (FBXL5) communicates cellular iron and oxygen availability by distinct mechanisms. *J. Biol. Chem.* **287,** 23710–23717
15. Thompson, J. W., Salahudeen, A. A., Chollangi, S., Ruiz, J. C., Brautigam, C. A., Makris, T. M., Lipscomb, J. D., Tomchick, D. R., and Bruick, R. K. (2012) Structural and molecular characterization of iron-sensing hemerythrin-like domain within F-box and leucine-rich repeat protein 5 (FBXL5). *J. Biol. Chem.* **287,** 7357–7365
16. Kitagawa, M., Hatakeyama, S., Shirane, M., Matsumoto, M., Ishida, N., Hattori, K., Nakamichi, I., Kikuchi, A., Nakayama, K., and Nakayama, K. (1999) An F-box protein, FWD1, mediates ubiquitin-dependent proteolysis of β-catenin. *EMBO J.* **18,** 2401–2410
17. Tahara-Hanaoka, S., Sudo, K., Ema, H., Miyoshi, H., and Nakauchi, H. (2002) Lentiviral vector-mediated transduction of murine CD34(−) hematopoietic stem cells. *Exp. Hematol.* **30,** 11–17
18. Kobayashi, Y., and Yonehara, S. (2009) Novel cell death by downregulation of eEF1A1 expression in tetraploids. *Cell Death Differ.* **16,** 139–150
19. Yumimoto, K., Matsumoto, M., Oyamada, K., Moroishi, T., and Nakayama, K. I. (2012) Comprehensive identification of substrates for F-box proteins by differential proteomics analysis. *J. Proteome Res.* **11,** 3175–3185
20. Nishiyama, M., Skoultchi, A. I., and Nakayama, K. I. (2012) Histone H1 recruitment by CHD8 is essential for suppression of the Wnt-β-catenin signaling pathway. *Mol. Cell. Biol.* **32,** 501–512
21. Mahler, H. R., and Elowe, D. G. (1954) Studies on metalloflavoproteins. II. The role of iron in diphosphopyridine nucleotide cytochrome *c* reductase. *J. Biol. Chem.* **210,** 165–179
22. Rotin, D., and Kumar, S. (2009) Physiological functions of the HECT family of ubiquitin ligases. *Nat. Rev. Mol. Cell Biol.* **10,** 398–409
23. Ang, X. L., and Wade Harper, J. (2005) SCF-mediated protein degradation and cell cycle control. *Oncogene* **24,** 2860–2870
24. Piccinelli, P., and Samuelsson, T. (2007) Evolution of the iron-responsive element. *RNA* **13,** 952–966
25. Thompson, J. W., and Bruick, R. K. (2012) Protein degradation and iron homeostasis. *Biochim. Biophys. Acta* **1823,** 1484–1490
26. Hochrainer, K., Mayer, H., Baranyi, U., Binder, B., Lipp, J., and Kroismayr, R. (2005) The human HERC family of ubiquitin ligases: novel members, genomic organization, expression profiling, and evolutionary aspects. *Genomics* **85,** 153–164
27. Ji, Y., Rebert, N. A., Joslin, J. M., Higgins, M. J., Schultz, R. A., and Nicholls, R. D. (2000) Structure of the highly conserved *HERC2* gene and of multiple partially duplicated paralogs in human. *Genome Res.* **10,** 319–329
28. Puffenberger, E. G., Jinks, R. N., Wang, H., Xin, B., Fiorentini, C., Sherman, E. A., Degrazio, D., Shaw, C., Sougnez, C., Cibulskis, K., Gabriel, S., Kelley, R. I., Morton, D. H., and Strauss, K. A. (2012) A homozygous missense mutation in HERC2 associated with global developmental delay and autism spectrum disorder. *Hum. Mutat.* **33,** 1639–1646
29. Bekker-Jensen, S., Rendtlew Danielsen, J., Fugger, K., Gromova, I., Nerstedt, A., Lukas, C., Bartek, J., Lukas, J., and Mailand, N. (2010) HERC2 coordinates ubiquitin-dependent assembly of DNA repair factors on damaged chromosomes. *Nat. Cell. Biol.* **12,** 80–86; sup pp 1–12
30. Kang, T. H., Lindsey-Boltz, L. A., Reardon, J. T., and Sancar, A. (2010) Circadian control of XPA and excision repair of cisplatin-DNA damage by

Downloaded from http://www.jbc.org/ at FUZOKU TOSHOKAN KYUSHU UNIV on November 17, 2014

cryptochrome and HERC2 ubiquitin ligase. *Proc. Natl. Acad. Sci. U.S.A.* **107,** 4890–4895
31. Wu, W., Sato, K., Koike, A., Nishikawa, H., Koizumi, H., Venkitaraman, A. R., and Ohta, T. (2010) HERC2 is an E3 ligase that targets BRCA1 for degradation. *Cancer Res.* **70,** 6384–6392
32. Ulrich, H. D., and Walden, H. (2010) Ubiquitin signalling in DNA replication and repair. *Nat. Rev. Mol. Cell Biol.* **11,** 479–489
33. Lill, R., and Mühlenhoff, U. (2008) Maturation of iron-sulfur proteins in eukaryotes: mechanisms, connected processes, and diseases. *Annu. Rev. Biochem.* **77,** 669–700
34. Berthelet, S., Usher, J., Shulist, K., Hamza, A., Maltez, N., Johnston, A., Fong, Y., Harris, L. J., and Baetz, K. (2010) Functional genomics analysis of the *Saccharomyces cerevisiae* iron responsive transcription factor Aft1 reveals iron-independent functions. *Genetics* **185,** 1111–1128

Downloaded from http://www.jbc.org/ at FUZUKU TOSHOKAN KYUSHU UNIV on November 17, 2014

From www.bloodjournal.org by guest on April 13, 2015. For personal use only.

Regular Article

LYMPHOID NEOPLASIA

p57 regulates T-cell development and prevents lymphomagenesis by balancing p53 activity and pre-TCR signaling

Akinobu Matsumoto, Shoichiro Takeishi, and Keiichi I. Nakayama

Department of Molecular and Cellular Biology, Medical Institute of Bioregulation, Kyushu University, Higashi-ku, Fukuoka, Fukuoka, Japan; and Core Research for Evolutional Science and Technology, Japan Science and Technology Agency, Kawaguchi, Saitama, Japan

Key Points

- Ablation of p57 in T cells blocks differentiation at an early developmental stage as a result of excessive activation of E2F.
- Additional ablation of E2F1 or p53 normalizes p57-deficiency phenotypes, but loss of both p57 and p53 eventually results in thymic lymphoma.

T cells are key components of the immune system, playing a central role in cell-mediated immunity. The sequential differentiation of T cells is associated with strict regulation of the cell cycle at each developmental stage. A balance between p53 activity and pre–T cell receptor (TCR) signaling regulates proliferation and differentiation decisions made by these cells. The relation between maintenance of this balance and the function of cell cycle regulators has remained largely unknown, however. We now show that mice with T cell–specific deficiency of the cyclin-dependent kinase inhibitor p57 manifest a differentiation block at the early stage of T cell maturation. Further genetic analysis showed that this defect is attributable to an imbalance between p53 activity and pre-TCR signaling caused by hyperactivation of the E2F-p53 pathway. Moreover, ablation of both p57 and p53 in T cells led to the development of aggressive thymic lymphomas with a reduced latency compared with that apparent for p53-deficient mice, whereas ablation of p57 alone did not confer susceptibility to this hematologic malignancy. Our results thus show that the p57-E2F-p53 axis plays a pivotal role in the proper development of T cells as well as in the prevention of lymphomagenesis. (*Blood.* 2014;123(22):3429-3439)

Introduction

Development and maturation of T lymphocytes in the thymus are essential for establishment of the peripheral immune system. Most immature T cells in the thymus initially neither express CD4 nor CD8, and they are therefore referred to as double-negative (DN) cells. This DN population can be further divided into 4 subsets (DN1 to DN4) defined by the sequential pattern of expression of CD44 and CD25: $CD44^+CD25^-$ (DN1), $CD44^+CD25^+$ (DN2), $CD44^-CD25^+$ (DN3), and $CD44^-CD25^-$ (DN4).[1] This maturation of T cells requires a sequence of events that is closely associated with rearrangement of the T-cell receptor (TCR) genes and signaling through this receptor. Activation of DN3 cells by pre-TCR–dependent signaling, referred to as the β-selection checkpoint, results in the generation of DN4 cells, which, in turn, differentiate into $CD4^+CD8^+$ (double-positive, or DP) cells via a transient $CD8^+$ (immature single-positive, or ISP) stage.[2] Subsequent downregulation of either CD4 or CD8 in DP cells gives rise to mature single-positive (SP) cells.[3] Differentiation of DN3/DN4 cells into DP cells is blocked by a defect in pre-TCR signaling resulting from genetic ablation of RAG1 or RAG2, DNA-dependent protein kinase (DNA-PK), or the CD3γ chain, and this block is prevented by concurrent loss of p53, suggesting that the β-selection checkpoint at the DN3 stage depends on a balance between pre-TCR signaling and p53 activation.[4-6] The precise mechanism of such p53 activation remains largely unclear, however.

Progression of the cell cycle is controlled by pairs of cyclins and cyclin-dependent kinases (CDKs).[7] CDKs normally inactivate the retinoblastoma protein (Rb) by hyperphosphorylation and thereby activate E2F transcription factors[8] that play a key role in cell cycle progression by regulating the transcription of genes that contribute to this process.[9] However, excessive E2F activity induces p53-dependent or p53-independent apoptosis in a manner dependent on cellular context.[10-13]

The activity of cyclin-CDK pairs is under the control of negative cell cycle regulators that belong to the Cip/Kip family of CDK inhibitors. Members of the Cip/Kip family, including $p21^{Cip1}$ (p21), $p27^{Kip1}$ (p27), and $p57^{Kip2}$ (p57), mainly target CDK2 and CDK4 (and CDK1 in some situations) for inhibition.[14] Among these members, p21 is dispensable for T-cell development.[15] Loss of p27 in mice results in an increase in overall animal growth as well as the development of pituitary tumors and hyperplasia of multiple organs including the thymus.[16-18] Unlike p21- or p27-deficient mice, mice lacking p57 die immediately after birth, manifesting severe developmental defects,[12,19,20] which has hindered the functional characterization of p57-deficient T cells.

In the present study, we established mice in which the p57 gene is conditionally disrupted in T lymphocytes. We found that acute inactivation of p57 results in a differentiation block at the transition from DN3 to DN4 cells. Further genetic analysis showed that this

Submitted October 11, 2013; accepted March 16, 2014. Prepublished online as *Blood* First Edition paper, March 20, 2014; DOI 10.1182/blood-2013-10-532390.

A.M. and S.T. contributed equally to this study.

The online version of this article contains a data supplement.

There is an Inside *Blood* Commentary on this article in this issue.

The publication costs of this article were defrayed in part by page charge payment. Therefore, and solely to indicate this fact, this article is hereby marked "advertisement" in accordance with 18 USC section 1734.

© 2014 by The American Society of Hematology

From www.bloodjournal.org by guest on April 13, 2015. For personal use only.

block is attributable to hyperactivation of E2F1 and p53, suggesting that p57 deficiency disrupts the balance between p53 activity and pre-TCR signaling. Finally, we observed that additional ablation of p53 on the p57-null background resulted in the development of thymic lymphoma, indicating that the p57-p53 axis also functions as a suppressor of this fatal hematologic malignancy.

Methods

Generation of conditional knockout mice

Female mice heterozygous for a floxed *p57* allele ($p57^{[+]/F}$ or $p57^{[F]/+}$) were crossed with male Lck-Cre or CD4-Cre (kindly provided by C. B. Wilson, University of Washington, Seattle, WA) transgenic mice.[21-23] Deletion of *p57* in the resulting offspring was detected by polymerase chain reaction (PCR) analysis of genomic DNA with the primers AM83 (5′-ATGAGCGTCTG TTAGGGACAGAC-3′), AM84 (5′-GACCAGACAGTCGAAATGGTTC C-3′), and AM85 (5′-GCCGCGGTGTTGTTGAAACTG-3′). Lck-Cre/$p57^{[+]/+}$ or CD4-Cre/$p57^{[+]/+}$ mice were studied as controls for Lck-Cre/$p57^{[+]/F}$ or CD4-Cre/$p57^{[+]/F}$ mice, respectively. Lck-Cre/$p57^{[+]/F}$ mice were also crossed with $E2f1^{-/-}$ (kindly provided by L. Yamasaki, Columbia University, New York, NY) or $p53^{-/-}$ (Taconic, Hudson, NY) mice. The animal ethics committee of Kyushu University approved all mouse experiments.

Flow cytometry and cell sorting

Antibodies to mouse CD4 (RM4-5), CD8α (53-6.7), CD25 (3C7), CD44 (IM7), TCRβ (H57-597), B220 (RA3-6B2), TER119, Gr-1 (RB6-8C59), Mac-1 (M1/70), and NK1.1 (PK136) were obtained from BD Biosciences (San Jose, CA). CD4, CD8, B220, TER119, Gr-1, Mac-1, and NK1.1 were used as lineage markers. For determination of bromodeoxyuridine (BrdU) incorporation in vivo, mice were injected intraperitoneally with BrdU (1 mg) twice, with a 2-hour interval between injections. The thymus was harvested 1 hour after the second injection, and BrdU incorporation was evaluated with a BrdU Flow kit (BD Biosciences). For assay of apoptosis, thymocytes or splenic T cells were stained for cell surface markers, further incubated for 15 minutes with annexin V (BD Biosciences), and then analyzed by flow cytometry. For determination of intracellular TCRβ expression, cells were fixed in 2% paraformaldehyde after surface staining to determine thymocyte subsets, and they were then stained with antibodies to TCRβ in phosphate-buffered saline (PBS) containing 0.5% saponin and 4% fetal bovine serum. Stained cells were analyzed and sorted with the use of FACSCalibur or FACSAria instruments (BD Biosciences).

Statistical analysis

Quantitative data are presented as means ± standard deviation (SD) and were analyzed with the 2-tailed Student *t* test. A P value of $< .05$ was considered statistically significant.

Additional procedures can be found in the supplemental Methods (available on the *Blood* Web site).

Results

p57 deficiency in T cells results in developmental arrest at the DN3-DN4 transition

To investigate the role of p57 in T-cell differentiation, we set out to delete the p57 gene specifically in T cells. Given that the *p57* locus undergoes genomic imprinting with only the maternal allele being expressed,[24] we crossed female mice heterozygous for a floxed allele ($p57^{[F]/+}$ or $p57^{[+]/F}$, with the symbols within square brackets representing the imprinted, inactive allele) with male mice harboring a *Cre* transgene under the control of the Lck gene promoter to yield Lck-Cre/$p57^{[+]/F}$ mice, in which the maternal *p57* allele would be expected to be deleted exclusively in the T-cell lineage. We confirmed that the floxed allele was indeed efficiently inactivated by Cre in T cells of these mice (Figure 1A).

The size and cell number for the thymus of Lck-Cre/$p57^{[+]/F}$ mice were markedly reduced compared with those for control (Lck-Cre/$p57^{[+]/+}$) mice (Figure 1B-C). Although the size of the spleen in Lck-Cre/$p57^{[+]/F}$ mice did not differ substantially from that in control animals (Figure 1D), the number of TCRβ-positive cells in the spleen of the mutant mice was also reduced significantly compared with that in controls (Figure 1E). Flow cytometric analysis of the thymus of Lck-Cre/$p57^{[+]/F}$ mice showed an increased proportion of DN cells and a reduced percentage of DP cells (Figure 1F). Further analysis of CD44 and CD25 expression in the DN subset showed an increase in the proportion of DN3 cells accompanied by a marked decrease in that of DN4 cells (Figure 1G), indicating that the transition from DN3 to DN4 was blocked by p57 ablation. This differentiation block in DN3 cells also reduced the absolute numbers of cells at later stages of differentiation (DN4, ISP, DP, CD4, or CD8 SP) in the mutant mice (Figure 1H).

To investigate the mechanism by which p57 deficiency results in the differentiation block at the DN3-DN4 transition, we examined DNA rearrangement at the TCRβ locus and the expression of pre-TCR components in the DN3 cell population, given that an increase in the percentage of DN3 cells is often observed as a result of a defect in β-selection. Analysis of genomic DNA for DJβ and V(D)Jβ rearrangement in DN3 cells showed no substantial differences between Lck-Cre/$p57^{[+]/F}$ and Lck-Cre/$p57^{[+]/+}$ mice (Figure 1I), suggesting that the genomic rearrangement underlying TCRβ chain production is intact in the p57-deficient cells. The frequency of DN3 cells positive for intracellular TCRβ expression also did not differ significantly between the 2 genotypes (Figure 1J-K). However, the proportion of DN4 cells positive for intracellular TCRβ expression was greatly reduced by p57 ablation (Figure 1J-K), providing additional evidence that the differentiation of p57-deficient T cells is blocked at the DN3-DN4 transition. We also found that the abundance of pTα mRNA was increased in p57-deficient DN3 cells compared with control cells (Figure 1L), suggesting that the loss of p57 in immature T cells results in a reduction in the number of these cells without impairment of pre-TCR signaling.

Loss of p57 in immature T cells impairs proliferation and induces apoptosis in association with Rb hyperphosphorylation

Mice in which the gene encoding pTα is inactivated manifest a marked, but incomplete, block in T-cell development at the transition from DN3 to DN4, as shown by a decrease in the proportion of proliferating DN4 cells.[25] Given that the timing of the differentiation block in p57-deficient T cells is almost identical to that in pTα-deficient mice, we examined the frequencies of proliferating cells and apoptotic cells among the DN3 and DN4 subsets in our mutant mice. Similar to the findings with pTα-deficient mice, the frequency of proliferating cells among the DN4 population of Lck-Cre/$p57^{[+]/F}$ mice was markedly decreased compared with that for control mice, whereas that for p57-deficient DN3 cells was reduced to a lesser extent (Figure 2A-B). Furthermore, we found that the frequency of apoptosis in DN4 cells was increased by p57 ablation (Figure 2C-D). These results suggested that a combination of cell cycle arrest and induction of apoptosis is responsible for the developmental defect in p57-deficient T cells. The sum of these effects of p57 deficiency thus

From www.bloodjournal.org by guest on April 13, 2015. For personal use only.

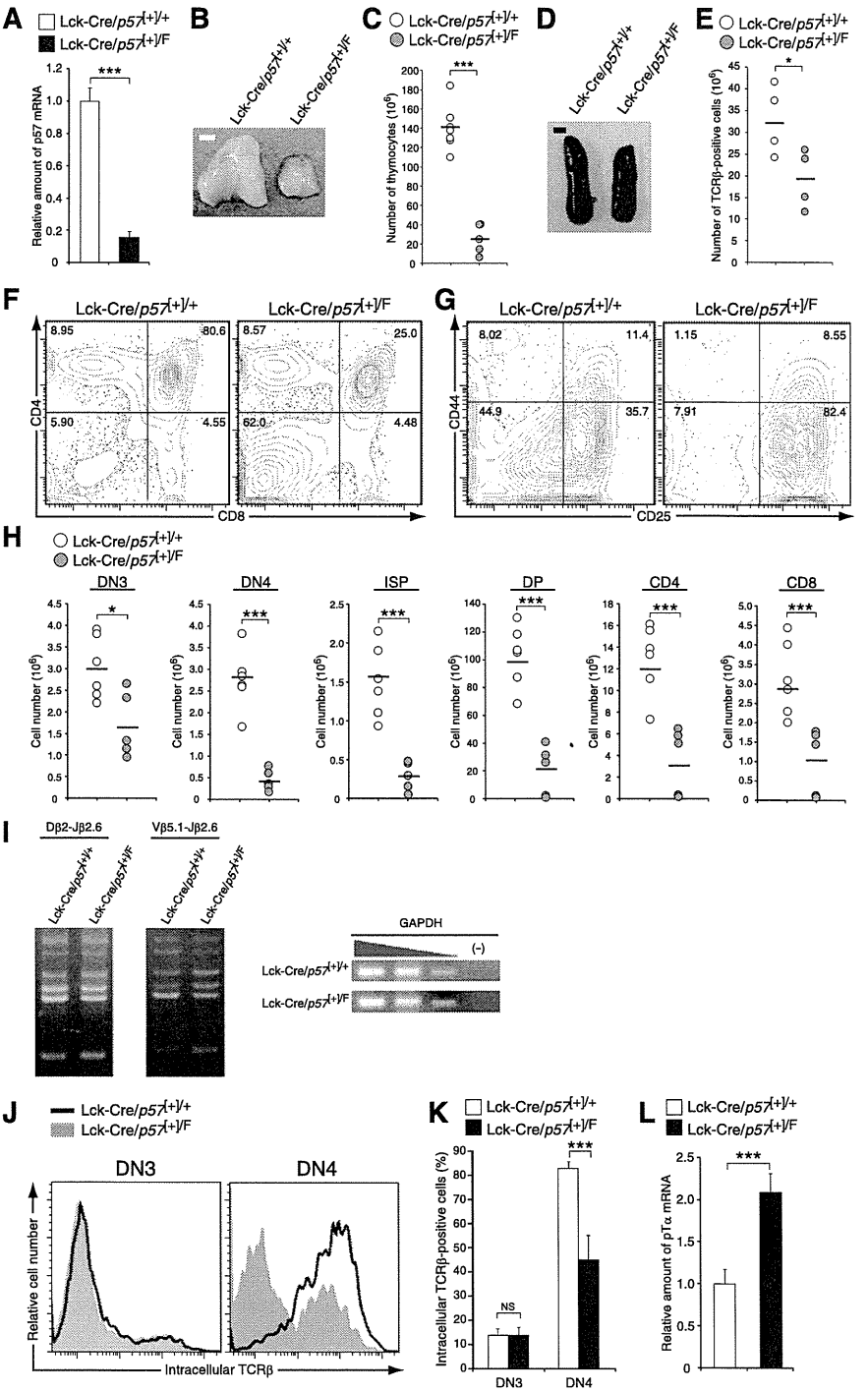

Figure 1. Loss of p57 in T cells results in a differentiation block at the DN3-DN4 transition and reduced thymic cellularity. (A) Reverse transcription (RT) and real-time PCR analysis of p57 mRNA in DN3 thymocytes from Lck-Cre/$p57^{[+]/+}$ and Lck-Cre/$p57^{[+]/F}$ mice at 8 weeks of age. Normalized data are expressed relative to the value for control mice and are means ± SD for 3 mice. ***$P < .005$. (B) Gross appearance of the thymus of Lck-Cre/$p57^{[+]/+}$ and Lck-Cre/$p57^{[+]/F}$ mice at 8 weeks of age. Scale bar, 2 mm. (C) Total number of thymocytes for individual Lck-Cre/$p57^{[+]/+}$ ($n = 7$) and Lck-Cre/$p57^{[+]/F}$ ($n = 5$) mice at 8 weeks of age. Bars indicate mean values. ***$P < .005$. (D) Gross appearance of the spleen of Lck-Cre/$p57^{[+]/+}$ and Lck-Cre/$p57^{[+]/F}$ mice at 8 weeks of age. Scale bar, 2 mm. (E) Number of TCRβ-positive cells among splenocytes of individual Lck-Cre/$p57^{[+]/+}$ and Lck-Cre/$p57^{[+]/F}$ mice at 8 weeks of age ($n = 4$). *$P < .05$. (F-G) Representative flow cytometric analysis of CD4 vs CD8 on thymocytes (F) and of CD44 vs CD25 on electronically gated lineage-negative DN thymocytes (G) from Lck-Cre/$p57^{[+]/+}$ and Lck-Cre/$p57^{[+]/F}$ mice at 8 weeks of age. Percentages of each fraction are indicated. (H) Absolute cell number for thymocyte subsets determined by flow cytometry ($n = 6$ for Lck-Cre/$p57^{[+]/+}$ and $n = 5$ for Lck-Cre/$p57^{[+]/F}$ mice). *$P < .05$, ***$P < .005$. (I) PCR analysis of genomic DNA for Dβ-to-Jβ rearrangement or V(D)Jβ recombination in DN3 cells from Lck-Cre/$p57^{[+]/+}$ and Lck-Cre/$p57^{[+]/F}$ mice at 8 weeks of age. Amplification of a GAPDH gene fragment was performed as an input control. (J) Representative histograms for flow cytometric analysis of intracellular TCRβ expression in DN3 and DN4 thymocytes from Lck-Cre/$p57^{[+]/+}$ and Lck-Cre/$p57^{[+]/F}$ mice at 8 weeks of age. (K) Determination of the proportion of cells positive for intracellular TCRβ expression as in panel J. Data are means ± SD for 4 mice. ***$P < .005$; NS, not significant. (L) RT and real-time PCR analysis of pTα mRNA in DN3 thymocytes from Lck-Cre/$p57^{[+]/+}$ and Lck-Cre/$p57^{[+]/F}$ mice at 8 weeks of age. Normalized data are expressed relative to the value for control mice and are means ± SD for 3 mice. ***$P < .005$.

likely accounts for the ~85% decrease in the number of DN4 cells in the mutant mice (Figure 1H).

We next investigated whether the Rb-E2F pathway is activated in p57-deficient T cells. Immunoblot (IB) analysis showed that the extent of Rb phosphorylation on Ser^{780} was increased in p57-deficient DN3 cells compared with control cells, whereas the extent of Rb phosphorylation at $Ser^{807/811}$ did not differ substantially between the 2 genotypes (Figure 2E). Examination of the expression of E2F target genes revealed that the expression levels of the genes for Mcm3, Cdc6, and Cdt1, all of which are related to cell cycle progression, were significantly increased in p57-deficient DN3 cells (Figure 2F). In addition, expression of the genes for ATM and ASPP1, which are E2F targets involved in apoptosis, was also markedly increased in these cells (Figure 2G). These results thus indicated that E2F activity was indeed increased by ablation of p57 in T cells.

p57 is not required for T-cell development at the DP stage

We next examined whether p57 is also indispensable for the development of mature T cells. To bypass the requirement for p57 at the earlier stage of T-cell development, we crossed p57-floxed mice

From www.bloodjournal.org by guest on April 13, 2015. For personal use only.

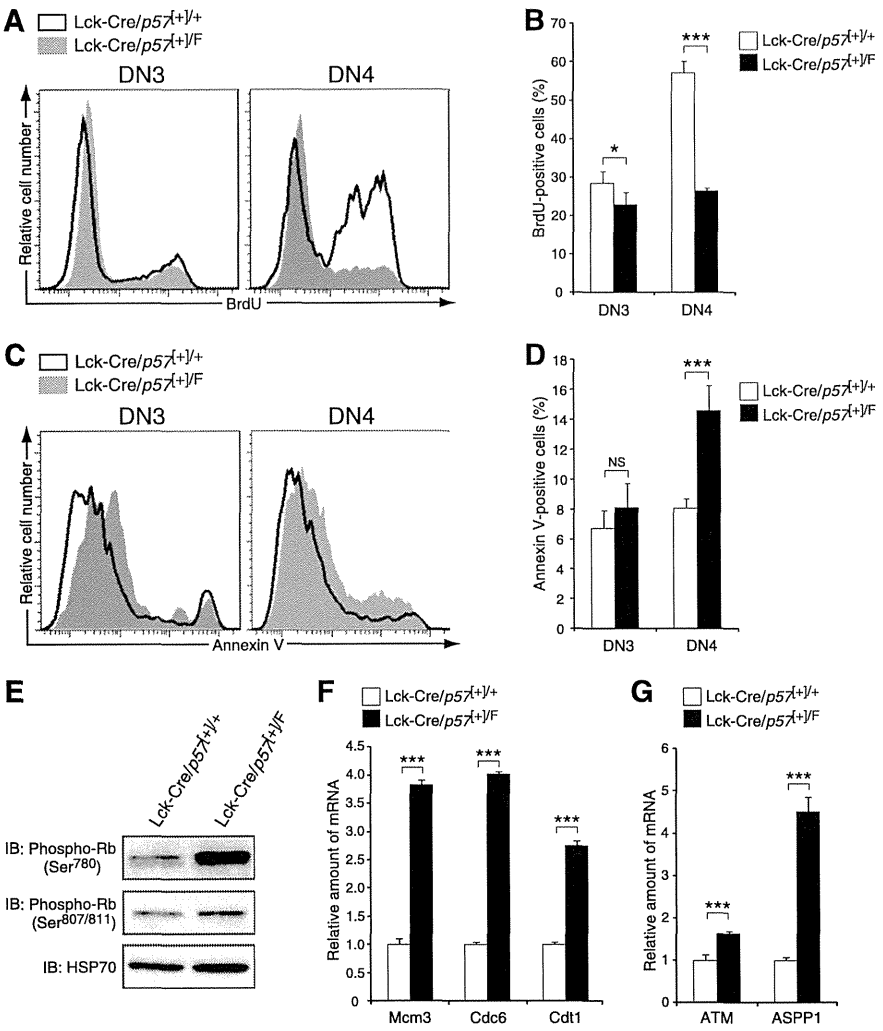

Figure 2. Loss of p57 results in a proliferative defect, induction of apoptosis, and excessive phosphorylation of Rb in thymocytes. (A) Representative flow cytometric histograms for BrdU staining in DN3 and DN4 thymocytes from Lck-Cre/$p57^{[+]/+}$ and Lck-Cre/$p57^{[+]/F}$ mice injected with BrdU at 8 weeks of age. (B) Determination of the proportion of cells positive for BrdU as in panel A. Data are means ± SD for 4 mice. $^{*}P < .05$, $^{***}P < .005$. (C) Representative histograms for annexin V staining in DN3 and DN4 thymocytes from Lck-Cre/$p57^{[+]/+}$ and Lck-Cre/$p57^{[+]/F}$ mice at 8 weeks of age. (D) Determination of the proportion of cells positive for annexin V staining as in panel C. Data are means ± SD for 4 mice. $^{***}P < .005$. (E) IB analysis of phosphorylated Rb in DN3 thymocytes from Lck-Cre/$p57^{[+]/+}$ and Lck-Cre/$p57^{[+]/F}$ mice at 8 weeks of age. HSP70 was examined as a loading control. (F-G) RT and real-time PCR analysis of Mcm3, Cdc6, and Cdt1 mRNAs (F) as well as of ATM and ASPP1 mRNAs (G) in DN3 thymocytes from Lck-Cre/$p57^{[+]/+}$ and Lck-Cre/$p57^{[+]/F}$ mice at 8 weeks of age. Normalized data are expressed relative to the corresponding value for control mice and are means ± SD for 3 mice. $^{***}P < .005$.

with CD4-Cre transgenic mice to generate CD4-Cre/$p57^{[+]/F}$ mice. Cre recombinase is not expressed in thymocytes of CD4-Cre mice until the late stage of DN cell development,[23] and consistent with this we detected a significant decrease in the abundance of p57 mRNA in DN4 cells but not in DN3 cells from CD4-Cre/$p57^{[+]/F}$ mice (Figure 3A). The size of the thymus and number of thymocytes did not differ between these mutant mice and control animals (Figure 3B-C). The numbers of DN3, DN4, DP, CD4 SP, and CD8 SP cells in CD4-Cre/$p57^{[+]/F}$ mice were also similar to those in control littermates, whereas the number of ISP cells was increased in the mutant animals (Figure 3D-E). These results thus indicated that p57 is dispensable for T-cell development after the DP stage.

p57-deficient mature T cells proliferate inefficiently in response to antigenic stimulation

Although the number of T cells in the thymus of CD4-Cre/$p57^{[+]/F}$ mice did not differ significantly from that for control mice, the number of TCRβ-positive cells in the spleen of CD4-Cre/$p57^{[+]/F}$ mice was significantly reduced (Figure 3F). To investigate the mechanism underlying this phenotype, we first examined BrdU incorporation and apoptosis in splenic T cells after mitogenic stimulation. The extent of BrdU incorporation was attenuated in splenic T cells from CD4-Cre/$p57^{[+]/F}$ mice at 36 hours after the onset of stimulation with antibodies to CD3ε (Figure 3G). Furthermore, the frequency of apoptotic cells was increased in splenic T cells from CD4-Cre/$p57^{[+]/F}$ mice after stimulation for 24 or 36 hours (Figure 3H). These results thus suggested that p57 is indispensable for the continuous proliferation of mature T cells in response to mitogenic stimulation, which is necessary for maintenance of the T cell population in peripheral lymphoid organs.

We next examined the possible contribution of the Rb-E2F pathway to the impaired proliferation of mature T cells from CD4-Cre/$p57^{[+]/F}$ mice. Whereas the extent of Rb phosphorylation on Ser^{780} was not greatly increased by p57 ablation in the absence or presence of anti-CD3ε stimulation, the extent of that at $Ser^{807/811}$ was increased in splenic T cells from CD4-Cre/$p57^{[+]/F}$ mice under both conditions (Figure 3I). This pattern of Rb phosphorylation on $Ser^{807/811}$ and Ser^{780} is opposite to that apparent for p57-deficient immature T cells (Figure 2E). In addition, the expression levels of the genes for Cdc6 and Cdt1 were significantly increased in the p57-deficient mature T cells, although those for the Mcm3, ATM, and ASPP1 genes did not differ between the 2 genotypes (Figure 3J-K). This pattern of E2F target gene expression differs from that apparent in thymocytes (Figure 2F-G), possibly as a result of the difference in the sites of Rb phosphorylation. Collectively, our data suggested that the reduction in the number of TCRβ-positive cells in the spleen of CD4-Cre/$p57^{[+]/F}$ mice is attributable, at least in part, to excessive activation of the Rb-E2F pathway in

From www.bloodjournal.org by guest on April 13, 2015. For personal use only.

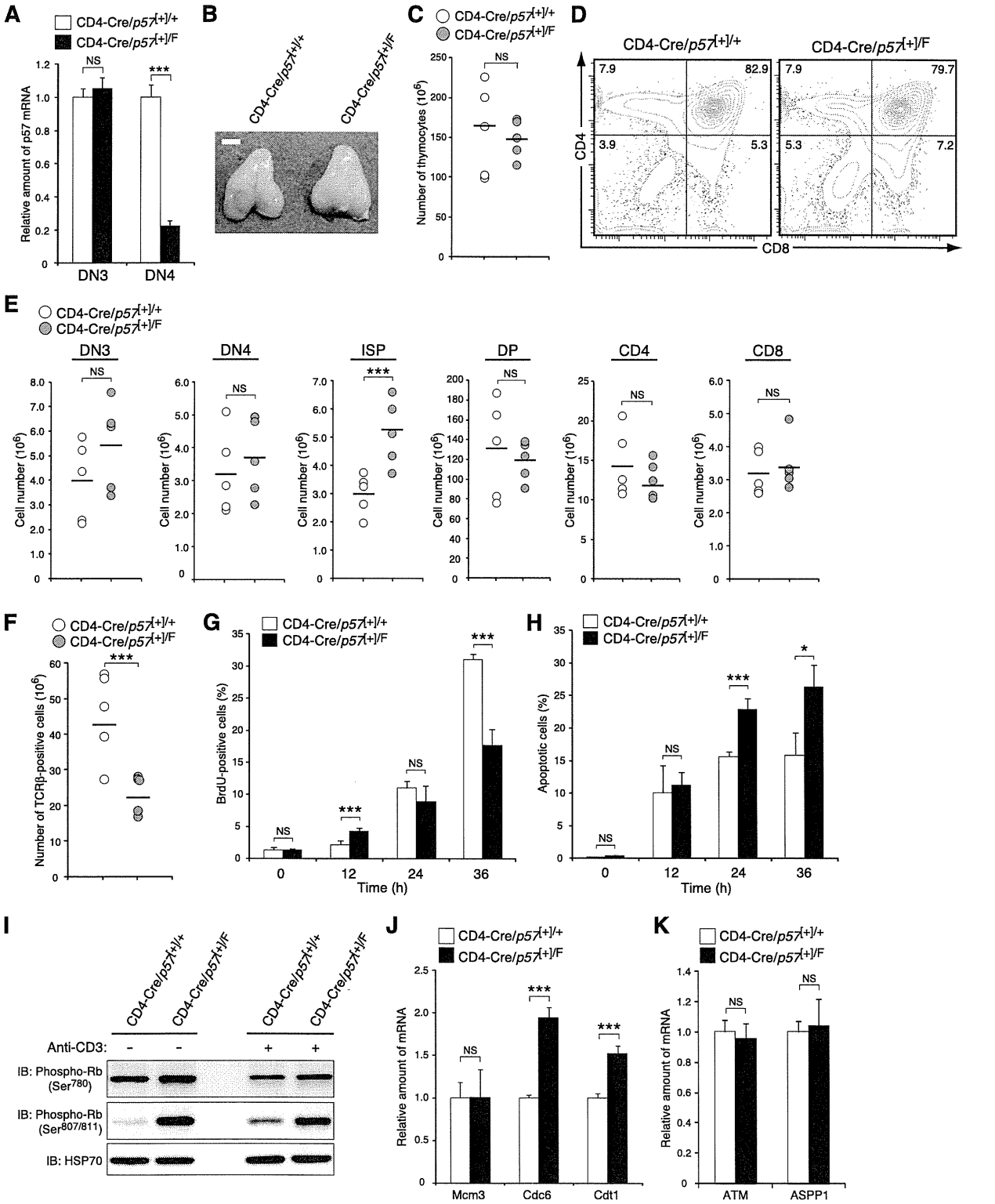

Figure 3. Ablation of p57 does not affect development of DP cells but impairs the proliferation and survival of antigen-stimulated mature T cells. (A) RT and real-time PCR analysis of p57 mRNA in DN3 and DN4 thymocytes from CD4-Cre/$p57^{[+]/+}$ and CD4-Cre/$p57^{[+]/F}$ mice at 8 weeks of age. Normalized data are expressed relative to the corresponding value for control mice and are means ± SD for 3 mice. ***$P < .005$. (B) Gross appearance of the thymus of CD4-Cre/$p57^{[+]/+}$ and CD4-Cre/$p57^{[+]/F}$ mice at 8 weeks of age. Scale bar, 2 mm. (C) Total number of thymocytes for individual CD4-Cre/$p57^{[+]/+}$ and CD4-Cre/$p57^{[+]/F}$ mice at 8 weeks of age ($n = 5$). (D) Representative flow cytometric analysis of CD4 vs CD8 on thymocytes from CD4-Cre/$p57^{[+]/+}$ and CD4-Cre/$p57^{[+]/F}$ mice at 8 weeks of age. Percentages of each fraction are indicated. (E) Absolute cell number for thymocyte subsets in individual CD4-Cre/$p57^{[+]/+}$ and CD4-Cre/$p57^{[+]/F}$ mice at 8 weeks of age ($n = 5$). ***$P < .005$. (F) Absolute number of TCRβ-positive cells among splenocytes from individual CD4-Cre/$p57^{[+]/+}$ and CD4-Cre/$p57^{[+]/F}$ mice at 8 weeks of age ($n = 5$). ***$P < .005$. (G) Splenic $CD3^+$ T cells from CD4-Cre/$p57^{[+]/+}$ and CD4-Cre/$p57^{[+]/F}$ mice at 8 weeks of age were stimulated with anti-CD3ε (5 μg/mL) for the indicated times and exposed to BrdU during the final 1 hour of incubation. They were then stained with anti-BrdU, and the percentage of BrdU-positive cells was determined by flow cytometry. Data are means ± SD for 3 mice. ***$P < .005$. (H) Splenic T cells stimulated as in panel G were stained with propidium iodide, and the percentage of sub-G_1 (apoptotic) cells was determined by flow cytometry. Data are means ± SD for 3 mice. *$P < .05$, ***$P < .005$. (I) IB analysis of phosphorylated Rb in splenic T cells stimulated (or not) as in panel G for 10 hours. (J-K) RT and real-time PCR analysis of Mcm3, Cdc6, and Cdt1 mRNAs (J) as well as of ATM and ASPP1 mRNAs (K) in splenic T cells stimulated as in panel G for 10 hours. Normalized data are expressed relative to the corresponding value for control mice and are means ± SD for 3 mice. ***$P < .005$.